Elastic Buckling and Vibration Analysis of FG Polymer Composite Plates Embedding Graphene Nanoplatelet Reinforcements in Thermal Environment

Journal:	*Mechanics of Advanced Materials and Structures*
Manuscript ID	Draft
Manuscript Type:	Manuscript
Date Submitted by the Author:	n/a
Complete List of Authors:	Fazzolari, Fiorenzo; University of Liverpool
Keywords:	Hierarchical plate theories, Eigenfrequencies, Critical buckling load, FG-GPLRC plates, Extended Haphin-Tsai model, Navier-type closed-form solution

Elastic Buckling and Vibration Analysis of FG Polymer Composite Plates Embedding Graphene Nanoplatelet Reinforcements in Thermal Environment

Fiorenzo A. Fazzolari[1,*]

University of Liverpool, School of Engineering, Brownlow Hill, Liverpool, L69 3GH, UK

Abstract

The present article proposes a comprehensive buckling and vibration analysis of functionally graded (FG) polymer composite plates reinforced with graphene platelets (GPLs). The effective material properties of the FG-GPLRC plates are accurately computed by using various ad-hoc micromechanical models. Several graphene nanoplatelets distribution patterns, within the polymer matrix, are investigated. The governing differential equations (GDEs) are derived by using Hamilton's principle combined with the method of the power series expansion of the displacement components and the Gauss theorem. They are, then, solved in an exact sense by using the Navier-type closed-form solution. Various case-studies are addressed to show the high level of accuracy of the proposed formulation. Moreover, the effect of length-to-thickness ratio, volume fraction, aspect ratio, variable kinematics as well as GPLs distribution pattern is discussed.

Keywords: Hierarchical plate theories, Eigenfrequencies, Critical Buckling load, FG-GPLRC plates, Extended Haphin-Tsai model, Navier-type closed-form solution.

1. Introduction

During the last two decades a significant amount of researchers belonging to the composite research community have focused their attention on the development and analysis of carbonaceous nano-fillers for advanced multifunctional composite materials. In particular, two different specific nano-fillers such as graphene (G) and carbon nanotubes (CNTs) have been thoroughly investigated.

*Corresponding author: Tel:+44 (0)151 794 5227
Email address: Fiorenzo.Fazzolari@liverpool.ac.uk (Fiorenzo A. Fazzolari)
[1]Department of Mechanical, Materials and Aerospace Engineering

Graphene is a two dimensional carbon based structure first introduced in 2004 [1]. It is a monolayer with atomic thickness which is composed of carbon atoms in a hexagonal pattern. It has extraordinary features such as high electrical and thermal conductivities, great mechanical strength, large specific surface area, and low manufacturing cost in comparison to other nanostructures. More specifically, compared with CNTs, they have a much bigger specific surface area which provides a much stronger bonding with the matrix hence, greatly enhanced load transfer capability. It has been both theoretically and experimentally observed that the addition of a very small amount of graphene nanoplatelet fillers (GNPLs) into the pristine polymer matrix can dramatically improve its mechanical properties [2, 3]. For instance, Rafiee et al. [4] demonstrated that by just adding the 0.1% weight fraction (wt.%) of GPLs, the strength and stiffness of the reinforced polymer composites are enhanced by the same degree achieved by adding 1.0 wt.% of CNTs. As a result of these outstanding properties, graphene is an excellent candidate for the reinforcement of the polymer composites.

Most of the investigation carried out on graphene is related to synthesis and fabrication techniques. Liang et al. [5] studied the molecular-level dispersion of graphene into poly(vinyl alcohol) and effective reinforcement of their nanocomposites. They found out that by using this technique the load transfer between the nanofiller graphene and matrix PVA and the mechanical properties of the graphene-based nanocomposite with molecule-level are significantly improved. Moreover, a 76% increase in tensile strength and a 62% improvement of Youngs modulus are achieved by addition of only 0.7 wt% of graphene oxide. By simply adding 1.8wt% of graphene oxide into poly (vinyl alcohol) (PVA) matrix and reducing graphene oxide into graphene nanosheets. Zhao et al. [6] fabricated graphene-reinforced PVA composite films with a 150% improvement in tensile strength and a nearly 10 times increase in Young's modulus. Wang et al. [7] dispersed GPLs with different sizes to epoxy resin using a sonication process followed by three-roll milling, and studied the effects of GPL sizes on the mechanical properties of GPL/epoxy nanocomposites. Their study indicated that a larger GPL size can significantly improve the tensile modulus but reduce the strength of the nanocomposites. Fang et al. [8] developed an efficient method to functionalize graphene nanosheets and manufactured polystyrene nanocomposites with the addition of 0.9 wt.% graphene nanosheets and achieved around 70% and 57% increase in tensile strength and Young's modulus, respectively.

However, due to the high costs related to the synthesis and fabrication of nanocomposites,

the use of advanced atomistic modelling such as the molecular dynamics (MD) has taken place. The latter has been widely used for the evaluation of the thermal and mechanical material properties of GPLRC plates. In this respect, the following articles are worth mentioning. Spanos et al. [9] estimated the elastic mechanical properties of graphene reinforced composites by using a multiscale finite element method in which the graphene is modeled based on its atomistic microstructure while the matrix is modeled by continuum finite element method. Lin and Shen [10] by virtue of melecular dynamic (MD) simulations derived the temperature dependent mechanical properties of graphene reinforced polymer nanocomposites. Khezerlou and Tahmasebipour [11] performed a molecular dynamic simulation of graphene-poly methyl methacrylate nano-composite. Roussou and Karatasos [12] dealt with molecular dynamics simulations of Graphene/poly(ethylene glycol) nanocomposites. Rahman and Haque [13] performed a molecular modeling of cross linked graphene-epoxy nanocomposites for characterization of elastic constants and interfacial properties. Zhang et al. [14] determined the load transfer of graphene/carbon nanotube/polyethylene hybrid nanocomposite via MD simulation. Rissanou and Harmandaris [15] studied the structure and dynamics of poly(- methylmethacrylate)/graphene systems through atomistic molecular dynamics simulations. Liu et al. [16] carried out MD simulation on interfacial mechanical properties of polymer nanocomposites with wrinkled graphene. Ansari et al. [17] derived the mechanical properties of defective single-layered graphene sheets via MD simulation. In addition, it is also worth mentioning some of recent articles focused on the modelling of GPLRC plates. Bending and free vibration analysis of functionally graded graphene versus carbon nanotube reinforced composite plates has been addressed by Marcia et al. [18]. Song at al. [19] dealt with the bending and buckling analyses of functionally graded polymer composite plates reinforced with graphene nanoplatelets. An isogeometric thermal buckling analysis of temperature dependent FG graphene reinforced laminated plates by using a NURBS formulation has been proposed by Mirzaei and Kiani [20]. Gholamia and Ansari [21] investigated the nonlinear harmonically excited vibration of third-order shear deformable functionally graded graphene platelet-reinforced composite rectangular plates by means of the variational differential quadrature (VDQ). Kiani [22] studied the isogeometric large amplitude free vibration of graphene reinforced laminated plates in thermal environment using NURBS formulation. Shen et al. [23] analysed the nonlinear vibration of functionally graded graphene-reinforced composite laminated plates in thermal environments. The nonlinear frequency of the FG-

GRC laminated plates have been determined by using the two-step perturbation technique. Song et al. [24] investigated the free and forced vibrations of functionally graded polymer composite plates reinforced with graphene nanoplatelets. The authors used the Navier-type closed form solution technique to obtain the natural frequencies and dynamic response of simply supported functionally graded GPL/polymer plates under a dynamic loading. Hosseini and Zhang [25] carried out a coupled thermoelastic analysis of an FG multilayer graphene platelets-reinforced nanocomposite cylinder using meshless GFD method and a modified micromechanical model.

In the present article the method of power series expansion of displacement components, extensively employed in the analysis of laminated composite and FGM beams, plates and shells [26–34] has been extended to provide a comprehensive eigenfrequency analysis of GNPLRC plates. In particular, the advanced quasi-3D plate theories with hierarchical capabilities have been developed and then validated and assessed against results available in literature. Highly stable trigonometric Ritz functions have been used in the approximation. A thorough convergence analysis has also been carried out. The modal characteristics of the GPLRC plates under investigation have been analysed while varying significant parameters such as length-to-thickness ratio, volume fraction, aspect ratio as well as GPLs distribution pattern. Finally, from all of the carried out numerical analyses some conclusions have been drawn.

2. Micromechanical models

Various micro-mechanical models able to determine the effective material properties of polymer composites reinforced with carbon-based fillers have been successfully developed. In the present article, for the evaluation of the Young's modulii and shear modulus the extended Halpin-Tsai model has been employed. In particular, the latter allow us to compute the latter in the following manner:

$$\begin{aligned} E_{11} &= \eta_1 \frac{1+\zeta_1 \xi_{11} \mathcal{V}_G}{1-\xi_{11}} E_m \\ E_{22} &= \eta_2 \frac{1+\zeta_2 \xi_{22} \mathcal{V}_G}{1-\xi_{22}} E_m \\ G_{12} &= \eta_3 \frac{1}{1-\xi_{12}} G_m \end{aligned} \tag{1}$$

where

$$\zeta_1 = 2\left(\frac{\ell_G}{\varrho_G}\right); \quad \zeta_2 = 2\left(\frac{d_G}{\varrho_G}\right); \tag{2}$$

Being ℓ_G, d_G and ϱ_G the length, the width and the effective thickness of the graphene sheet. Moreover,

$$\xi_{11} = \frac{\frac{E_{11}^G}{E_m} - 1}{\frac{E_{11}^G}{E_m} + \zeta 1}; \quad \xi_{22} = \frac{\frac{E_{22}^G}{E_m} - 1}{\frac{E_{22}^G}{E_m} + \zeta 2}; \quad \xi_{12} = \frac{\frac{G_{12}^G}{G_m} - 1}{\frac{G_{12}^G}{G_m}} \tag{3}$$

where E_{11}^G, E_{22}^G and G_{12}^G are the Young's moduli and the shear modulus of the graphene sheet, and E_m and G_m the corresponding ones of the polymeric matrix. The quantities $\mathcal{V}_G$ and $\mathcal{V}_m$ represent the volume fraction of the GPLs and the polymeric matrix, respectively, and they are related by the equation $\mathcal{V}_G(z) + \mathcal{V}_m(z) = 1$. Similarly to other types of carbonaceous nanofillers, a crucial point is the bonding between the reinforcement and the matrix. In real life this bonding is less than perfect and phenomena such as strain gradient, nonlocal effect, intermolecular coupled stress effects occur. In order to take into account the latter, the graphene efficiency parameters η_i with $i = 1, 2, 3$ are introduced. These parameters are determined by matching the results coming from the micromechanical model with those obtained by using the molecular dynamics (MD) simulations [10, 23] and they also represent the extension of the classical Halpin-Tsai model.

The thermal expansion coefficients of the composite media are evaluated according to the Schapery model [35]. The latter is also extensively used to obtain the thermal expansion coefficients of CNTs-reinforced composites.

$$\begin{aligned} \alpha_{11}(z,T) &= \frac{V_G(z)\, E_{11}^G(T)\, \alpha_{11}^G(T) + V_m(z)\, E_m(T)\, \alpha^m(T)}{V_G(z)\, \alpha_{11}^G(T) + V_m(z)\, \alpha^m(T)}; \\ \alpha_{22}(z,T) &= \left(1 + \nu_{12}^G\right) V_G(z)\, \alpha_{22}^G + \left(1 + \nu_{12}^m\right) V_m(z)\, \alpha_m(T) - \nu_{12}(z)\, \alpha_{11}^G(T) \end{aligned} \tag{4}$$

where α_{11}^G, α_{22}^G and α^m are the thermal expansion coefficients of the GPL and the matrix, respectively. It should be borne in mind that in the present article the materials are considered temperature-dependent. Thus, the Young's moduli, the shear modulus and the thermal expansion coefficients, of both matrix and GPLs, are function of temperature T and the plate-thickness coordinate z. In particular, the matrix is made up of Poly Methyl Methacrylate (PMMA) whose material properties have a temperature dependency according to the following equation:

$$\begin{aligned} &E_m(T) = (3.52 - 0.0034\,T)\ GPa; \ \alpha_m(T) = 45\,(1 + 0.0005\,\Delta T) \times \frac{10^{-6}}{K}; \ \rho_m = 1150\,\frac{Kg}{m^3}; \\ &\nu_m = 0.34 \end{aligned} \tag{5}$$

The dependency of the GPLs to the temperature is given in Table 1.

Finally, the Poisson's ratio and mass density of the composite media may be expressed easily

according to the conventional Voigt's rule of mixtures (ROM) in terms of the Poisson ratio and mass density of the constituents as follows

$$\begin{aligned} \nu_{12} &= \mathcal{V}_G\, \nu_{12}^G + \mathcal{V}_m\, \nu_m \\ \rho &= \mathcal{V}_G\, \rho^G + \mathcal{V}_m\, \rho_m \end{aligned} \tag{6}$$

ρ_m and ρ_G are the densities of the matrix and graphene platelets, respectively

3. Geometric and constitutive relations

The nomenclature and geometry of the GPLRC plate are shown in Fig. 1. In addition to that, it is useful to recall that, the reference plane, often referred to as plate middle-surface, which lies in the plane (xy) is named Ω whilst the z coordinate is referred to as thickness coordinate. According to the classical nomenclature used in literature, the length of the plate in the x and y-direction is indicated by a and b, respectively, while the thickness dimension is denoted as h. Consistently to the reference coordinate system the stress and strain vectors are indicated as follows

$$\boldsymbol{\sigma} = \left\{ \begin{array}{cccccc} \sigma_{xx} & \sigma_{yy} & \tau_{xy} & \tau_{xz} & \tau_{yz} & \sigma_{zz} \end{array} \right\}^T, \quad \boldsymbol{\varepsilon} = \left\{ \begin{array}{cccccc} \varepsilon_{xx} & \varepsilon_{yy} & \gamma_{xy} & \gamma_{xz} & \gamma_{yz} & \varepsilon_{zz} \end{array} \right\}^T \tag{7}$$

The strain-displacement relations are

$$\boldsymbol{\varepsilon} = \mathbf{D}\mathbf{u} \tag{8}$$

where $\mathbf{D}$ and $\mathbf{u}$ are a differential matrix operator and the displacement vector, defined as follows

$$\mathbf{D} = \begin{bmatrix} \frac{\partial}{\partial x} & 0 & 0 \\ 0 & \frac{\partial}{\partial y} & 0 \\ \frac{\partial}{\partial y} & \frac{\partial}{\partial x} & 0 \\ \frac{\partial}{\partial z} & 0 & \frac{\partial}{\partial x} \\ 0 & \frac{\partial}{\partial z} & \frac{\partial}{\partial y} \\ 0 & 0 & \frac{\partial}{\partial z} \end{bmatrix}, \quad \mathbf{u} = \left\{ \begin{array}{c} u_x \\ u_y \\ u_z \end{array} \right\} \tag{9}$$

The 3D constitutive equations related to thermoelastic problem can be written in the following compact form,

$$\boldsymbol{\sigma} = \mathbf{C}\,(z,T)\,\boldsymbol{\varepsilon} - \boldsymbol{\Xi}\,(z,T)\;\Delta T \tag{10}$$

where ΔT is the temperature variation and $\boldsymbol{\Xi}$ is the thermoelastic coupling coefficient which is given as

$$\boldsymbol{\Xi}\,(z,T) = \mathbf{C}\,(z,T)\;\boldsymbol{\alpha}\,(z,T) \tag{11}$$

$\boldsymbol{\alpha}$ is the vector including the coefficients of thermal expansion and assumes the following form

$$\boldsymbol{\alpha}(z,T) = \left\{ \begin{array}{cccccc} \alpha_{11}(z,T) & \alpha_{22}(z,T) & 0 & 0 & 0 & \alpha_{33}(z,T) \end{array} \right\}^T \tag{12}$$

and $\mathbf{C}$ is the constitutive matrix,

$$\mathbf{C}(z,T) = \left[\begin{array}{cccccc} C_{11}(z,T) & C_{12}(z,T) & 0 & 0 & 0 & C_{13}(z,T) \\ C_{12}(z,T) & C_{22}(z,T) & 0 & 0 & 0 & C_{23}(z,T) \\ 0 & 0 & C_{66}(z,T) & 0 & 0 & 0 \\ 0 & 0 & 0 & C_{44}(z,T) & 0 & 0 \\ 0 & 0 & 0 & 0 & C_{55}(z,T) & 0 \\ C_{31}(,T) & C_{32}(z,T) & 0 & 0 & 0 & C_{33}(z,T) \end{array} \right] \tag{13}$$

where the explicit expression of $\alpha_{ii}(z,T)$ and $C_{ij}(z,T)$ in terms of Young's modulii and Poisson's ratios can be found in standard composite materials textbooks [36, 37] and represent the effective elastic coefficients. It should also be noted that the latter have been derived in Sec 2.

4. Hierarchical plate models

The latest and most advanced structural theories used in the modelling of plate structural components are based on the Lagrangian Mechanics (LM). In this respect, a general and structured manner of development of hierarchical theories is the use of the method of power series expansion of the displacement components. The intrinsically generalised nature of this approach, derives by the fact that, at least in principled, any polynomial, non-polynomial and hybrid thickness functions can be successfully employed to describe the axiomatic assumptions of the through-the-thickness plate directions kinematics. This methodology will be employed in this article, it also represents a significant improvement of the classical theories first proposed by Kircchoff [38], Love [39, 40], Reissner [41] and Mindlin [41, 42], and based on the Newtonian Mechanics (NM).

More specifically, the methodology consists in the generation of theoretically infinite displacement fields via arbitrary expansions of each displacement component within the displacement field. Of course, the expansion order are opportunly selected according to consideration based on the computational cost and the required level of accuracy. This approach was already theorised by Washitsu [43] and then extensively used in the last three decades by Matsunaga [44]

and Carrera [45, 46], amongst others. The full exploitation of this revolutionary approach in the modelling of structures has only been possible due to the significant enhancement in the computer performances.

According to this, relatively new, approach the most general displacement field can be given as follows

$$\begin{aligned} u_x(x,y,z,t) &= \sum_{\tau_{u_x}=1}^{N_{u_x}} F_{\tau_{u_x}}(z)\, u_{x\tau_{u_x}}(x,y,t) \\ u_y(x,y,z,t) &= \sum_{\tau_{u_y}=1}^{N_{u_y}} F_{\tau_{u_y}}(z)\, u_{y\tau_{u_y}}(x,y,t) \\ u_z(x,y,z,t) &= \sum_{\tau_{u_z}=1}^{N_{u_z}} F_{\tau_{u_z}}(z)\, u_{z\tau_{u_z}}(x,y,t) \end{aligned} \tag{14}$$

where N_{u_x}, N_{u_y} and N_{u_z} are the orders of expansion of the in-plane and out-of-plane displacement components, respectively. The functions $F_{\tau_{u_x}}$, $F_{\tau_{u_y}}$, $F_{\tau_{u_z}}$ are usually referred to as the thickness functions. They can be generic functions of the plate-thickness coordinate. Their purpose is to accurately describe the plate kinematics through-the-thickness direction. To this aim, in the present investigation Taylor polynomials have been chosen, and an example of the displacement field with expansion orders $N_{u_x} = 5$, $N_{u_y} = 7$ and $N_{u_z} = 3$ is provided below:

$$\begin{aligned} u_x &= u_{x_0} + z\,u_{x_1} + z^2\,u_{x_2} + z^3\,u_{x_3} + z^4\,u_{x_4} + z^5\,u_{x_5} \\ u_y &= u_{y_0} + z\,u_{y_1} + z^2\,u_{y_2} + z^3\,u_{y_3} + z^4\,u_{y_4} + z^5\,u_{y_5} + z^6\,u_{y_6} + z^7\,u_{y_7} \\ u_z &= u_{z_0} + z\,u_{z_1} + z^2\,u_{z_2} + z^3\,u_{z_3} \end{aligned} \tag{15}$$

Finally, the functions $u_{x\tau_{u_x}}$, $u_{y\tau_{u_y}}$, $u_{z\tau_{u_z}}$ represent the displacement vector components.

5. Theoretical Formulation

In the derivation of what follows Hamilton's principle (HP) is employed to derive the governing equations in their weak form. The solution is then sought by using the Hierarchical Trigonometric Ritz Formulation (HTRF). In its classical form HP can be written as

$$\int_{t_1}^{t^2} \delta\mathcal{L}\,\mathrm{d}t = 0 \tag{16}$$

where t_1 and t_2 are the initial and the generic instant of time; $\mathcal{L}$ is the Lagrangian which assumes the following form

$$\mathcal{L} = T - \Pi \quad \text{where} \quad \Pi = \Phi_e + \Phi_\sigma \tag{17}$$

T is the kinetic energy and Π is the total potential energy of the system; Φ_e and Φ_σ are the potential strain energy and the potential energy due to the thermal and/or mechanical initial stresses, respectively. HP can be alternatively written in terms of displacements as follows

$$\begin{aligned}
\int_{t_1}^{t^2} \Bigg\{ \int_\Omega \int_{\mathcal{A}_z} \Big[& C_{11}(z,T)\,\delta u_{x,x}\,u_{x,x} + C_{66}(z,T)\,\delta u_{x,y}\,u_{x,y} + C_{55}(z,T)\,\delta u_{x,z}\,u_{x,z} + \\
& C_{16}(z,T)\,\delta u_{x,y}\,u_{x,x} + C_{16}(z,T)\,\delta u_{x,y}\,u_{x,y} + C_{12}(z,T)\,\delta u_{x,x}\,u_{y,y} + \\
& C_{66}(z,T)\,\delta u_{x,y}\,u_{y,x} + C_{16}(z,T)\,\delta u_{x,x}\,u_{y,x} + C_{26}(z,T)\,\delta u_{x,y}\,u_{y,y} + \\
& C_{45}(z,T)\,\delta u_x\,u_y + C_{13}(z,T)\,\delta u_{x,x}\,u_{z,z} + C_{55}(z,T)\,\delta u_{x,z}\,u_{z,x} + \\
& C_{36}(z,T)\,\delta u_{x,y}\,u_z + C_{45}(z,T)\,\delta u_x\,u_{z,y} + C_{12}(z,T)\,\delta u_{y,x}\,u_{x,y} + \\
& C_{66}(z,T)\,\delta u_{y,y}\,u_{x,x} + C_{16}(z,T)\,\delta u_{y,x}\,u_{x,x} + C_{26}(z,T)\,\delta u_{y,y}\,u_{x,y} + \\
& C_{45}(z,T)\,\delta u_y\,u_x + C_{22}(z,T)\,\delta u_{y,y}\,u_{y,y} + C_{66}(z,T)\,\delta u_{y,x}\,u_{y,x} + \\
& C_{44}(z,T)\,\delta u_{y,z}\,u_{y,z} + C_{26}(z,T)\,\delta u_{y,y}\,u_{y,x} + C_{26}(z,T)\,\delta u_{y,x}\,u_{y,y} + \\
& C_{44}(z,T)\,\delta u_{y,y}\,u_{z,z} + C_{23}(z,T)\,\delta u_{y,z}\,u_{z,y} + C_{36}(z,T)\,\delta u_{y,z}\,u_z + \\
& C_{45}(z,T)\,\delta u_y\,u_{z,x} + C_{13}(z,T)\,\delta u_{z,x}\,u_{x,z} + C_{55}(z,T)\,\delta u_{z,z}\,u_{x,x} + \\
& C_{36}(z,T)\,\delta u_z\,u_{x,y} + C_{45}(z,T)\,\delta u_{z,y}\,u_x + C_{44}(z,T)\,\delta u_{z,y}\,u_{y,z} + \\
& C_{23}(z,T)\,\delta u_{z,z}\,u_{y,y} + C_{36}(z,T)\,\delta u_z\,u_{y,x} + C_{45}(z,T)\,\delta u_{z,x}\,u_y + \\
& C_{44}(z,T)\,\delta u_{z,z}\,u_{z,z} + C_{55}(z,T)\,\delta u_{z,x}\,u_{z,x} + C_{33}(z,T)\,\delta u_{z,y}\,u_{z,y} + \\
& C_{45}(z,T)\,\delta u_{z,y}\,u_{z,x} + C_{45}(z,T)\,\delta u_{z,x}\,u_{z,y} \Big] \mathrm{d}\Omega\,\mathrm{d}z + \\
\int_\Omega \int_{\mathcal{A}_z} \Big[& \tilde{\sigma}_{xx_0}\,\delta u_{x,x}\,u_{x,x} + \tilde{\sigma}_{yy_0}\,\delta u_{x,y}\,u_{x,y} + \tilde{\tau}_{xy_0}\,\delta u_{x,x}\,u_{x,y} + \\
& \tilde{\sigma}_{xx_0}\,\delta u_{y,x}\,u_{y,x} + \tilde{\sigma}_{yy_0}\,\delta u_{y,y}\,u_{y,y} + \tilde{\tau}_{xy_0}\,\delta u_{y,x}\,u_{y,y} + \\
& \tilde{\sigma}_{xx_0}\,\delta u_{z,x}\,u_{z,x} + \tilde{\sigma}_{yy_0}\,\delta u_{z,y}\,u_{z,y} + \tilde{\tau}_{xy_0}\,\delta u_{z,x}\,u_{z,y} \Big] \mathrm{d}\Omega\,\mathrm{d}z + \\
\int_\Omega \int_{\mathcal{A}_z} & \Big[\rho\left(\delta\dot{u}_x\,\dot{u}_x + \delta\dot{u}_y\,\dot{u}_y + \delta\dot{u}_z\,\dot{u}_z\right) \Big] \mathrm{d}\Omega\,\mathrm{d}z \Bigg\} \mathrm{d}t = 0
\end{aligned} \tag{18}$$

where ρ is the material density; $\tilde{\sigma}_{xx_0}$, $\tilde{\sigma}_{yy_0}$ and $\tilde{\tau}_{xy_0}$ are the thermo-mechanical initial stresses. For the sake of completeness, the explicit derivation of thermal stresses generated due to the thermal environment are given in Appendix 7. The $,x$; $,y$; and $,z$ represent derivative with respect to these variables, and $\dot{()}$ indicates the time derivative. It should also be noted that in Eq. (18), it has been highlighted the dependency of the effective elastic coefficients from both the thickness coordinate z and the temperature T. The former is due to the FG-GPLs distributions the latter is related to the temperature-dependency of both matrix (see Eqs. (5)) and GPLs (see Table (1)).

Governing differential equations

In what follows the Governing Differential Equations (GDEs) and the variationally consistent Boundary Conditions (BCs) are derived by using Hamilton's principles (see Eq. (16)) and the Gauss Theorem. The latter is given as follows

$$\int_{\Omega} \frac{\partial\left(\delta u\right)}{\partial \zeta}\, v \,\mathrm{d}\Omega = \int_{\Gamma_m} \left(\delta u\right)\, v\, \hat{n}_{\zeta} \,\mathrm{d}\Gamma_m - \int_{\Omega} \left(\delta u\right) \frac{\partial v}{\partial \zeta} \,\mathrm{d}\Omega \tag{19}$$

where u and v represent two displacement variables; $\zeta = x, y, z$; Γ_m is the boundary accounting for the mechanical boundary conditions and $\hat{n}_{\zeta}$ are the direction cosines. By applying Eq. (19) at Eq. (18) the GDEs and the BCs are derived. The former can be written in compact form as

$$\begin{aligned}
\delta \left\{ \begin{array}{c} u_{x_{\tau_{u_x}}} \\ u_{y_{\tau_{u_y}}} \\ u_{z_{\tau_{u_z}}} \end{array} \right\} : \Bigg(& \left[\begin{array}{ccc} \mathcal{D}_{u_x\, u_x}^{\tau_{u_x}\, s_{u_x}} & \mathcal{D}_{u_x\, u_y}^{\tau_{u_x}\, s_{u_y}} & \mathcal{D}_{u_x\, u_z}^{\tau_{u_x}\, s_{u_z}} \\ \mathcal{D}_{u_y\, u_x}^{\tau_{u_y}\, s_{u_x}} & \mathcal{D}_{u_y\, u_y}^{\tau_{u_y}\, s_{u_y}} & \mathcal{D}_{u_y\, u_z}^{\tau_{u_y}\, s_{u_z}} \\ \mathcal{D}_{u_z\, u_x}^{\tau_{u_z}\, s_{u_x}} & \mathcal{D}_{u_z\, u_y}^{\tau_{u_z}\, s_{u_y}} & \mathcal{D}_{u_z\, u_z}^{\tau_{u_z}\, s_{u_z}} \end{array} \right] - \\
& \left[\begin{array}{ccc} \delta_{vK}\, \mathcal{S}_{u_x\, u_x}^{\tau_{u_x}\, s_{u_x}} & 0_{\tau_{u_x}\, s_{u_y}} & 0_{\tau_{u_x}\, s_{u_z}} \\ 0_{\tau_{u_y}\, s_{u_x}} & \delta_{vK}\, \mathcal{S}_{u_y\, u_y}^{\tau_{u_y}\, s_{u_y}} & 0_{\tau_{u_y}\, s_{u_z}} \\ 0_{\tau_{u_z}\, s_{u_x}} & 0_{\tau_{u_z}\, s_{u_y}} & \mathcal{S}_{u_z\, u_z}^{\tau_{u_x}\, s_{u_x}} \end{array} \right] \Bigg) \left\{ \begin{array}{c} u_{x_{s_{u_x}}} \\ u_{y_{s_{u_y}}} \\ u_{z_{s_{u_z}}} \end{array} \right\} + \\
& \left[\begin{array}{ccc} \mathcal{M}_{u_x\, u_x}^{\tau_{u_x}\, s_{u_x}} & 0_{\tau_{u_x}\, s_{u_y}} & 0_{\tau_{u_x}\, s_{u_z}} \\ 0_{\tau_{u_y}\, s_{u_x}} & \mathcal{M}_{u_y\, u_y}^{\tau_{u_y}\, s_{u_y}} & 0_{\tau_{u_y}\, s_{u_z}} \\ 0_{\tau_{u_z}\, s_{u_x}} & 0_{\tau_{u_z}\, s_{u_y}} & \mathcal{M}_{u_z\, u_z}^{\tau_{u_z}\, s_{u_z}} \end{array} \right] \left\{ \begin{array}{c} \ddot{u}_{x_{s_{u_x}}} \\ \ddot{u}_{y_{s_{u_y}}} \\ \ddot{u}_{z_{s_{u_z}}} \end{array} \right\} = \left\{ \begin{array}{c} 0_{s_{u_x}} \\ 0_{s_{u_y}} \\ 0_{s_{u_z}} \end{array} \right\}
\end{aligned} \tag{20}$$

while the latter (Neumann-type BCs) on Γ can be written as follows

$$\begin{aligned}
\delta \left\{ \begin{array}{c} u_{x_{\tau_{u_x}}} \\ u_{y_{\tau_{u_y}}} \\ u_{z_{\tau_{u_z}}} \end{array} \right\} : & \left[\begin{array}{ccc} \Pi_{u_x\, u_x}^{\tau_{u_x}\, s_{u_x}} - \Sigma_{u_x\, u_x}^{\tau_{u_x}\, s_{u_x}} & \Pi_{u_x\, u_y}^{\tau_{u_x}\, s_{u_y}} & \Pi_{u_x\, u_z}^{\tau_{u_x}\, s_{u_z}} \\ \Pi_{u_y\, u_x}^{\tau_{u_y}\, s_{u_x}} & \Pi_{u_y\, u_y}^{\tau_{u_y}\, s_{u_y}} - \Sigma_{u_y\, u_y}^{\tau_{u_y}\, s_{u_y}} & \Pi_{u_y\, u_z}^{\tau_{u_y}\, s_{u_z}} \\ \Pi_{u_z\, u_x}^{\tau_{u_z}\, s_{u_x}} & \Pi_{u_z\, u_y}^{\tau_{u_z}\, s_{u_y}} & \Pi_{u_z\, u_z}^{\tau_{u_z}\, s_{u_z}} - \Sigma_{u_z\, u_z}^{\tau_{u_z}\, s_{u_z}} \end{array} \right] \left\{ \begin{array}{c} u_{x_{s_{u_x}}} \\ u_{y_{s_{u_y}}} \\ u_{z_{s_{u_z}}} \end{array} \right\} = \\
& \left[\begin{array}{ccc} \Pi_{u_x\, u_x}^{\tau_{u_x}\, s_{u_x}} - \Sigma_{u_x\, u_x}^{\tau_{u_x}\, s_{u_x}} & \Pi_{u_x\, u_y}^{\tau_{u_x}\, s_{u_y}} & \Pi_{u_x\, u_z}^{\tau_{u_x}\, s_{u_z}} \\ \Pi_{u_y\, u_x}^{\tau_{u_y}\, s_{u_x}} & \Pi_{u_y\, u_y}^{\tau_{u_y}\, s_{u_y}} - \Sigma_{u_y\, u_y}^{\tau_{u_y}\, s_{u_y}} & \Pi_{u_y\, u_z}^{\tau_{u_y}\, s_{u_z}} \\ \Pi_{u_z\, u_x}^{\tau_{u_z}\, s_{u_x}} & \Pi_{u_z\, u_y}^{\tau_{u_z}\, s_{u_y}} & \Pi_{u_z\, u_z}^{\tau_{u_z}\, s_{u_z}} - \Sigma_{u_z\, u_z}^{\tau_{u_z}\, s_{u_z}} \end{array} \right] \left\{ \begin{array}{c} \bar{u}_{x_{s_{u_x}}} \\ \bar{u}_{y_{s_{u_y}}} \\ \bar{u}_{z_{s_{u_z}}} \end{array} \right\}
\end{aligned} \tag{21}$$

In Eq. (20) the tracer δ_{wK} has been introduced in order to retain and/or discard the full nonlinear terms. In the latter case, namely $\delta_{wK} = 0$, the von kármán approximation is assumed. The nine components of the fundamental primary differential stiffness nucleus $\mathbf{D}^{\tau s}$

are given, in their explicit form, as follows

$$\begin{aligned}
\mathcal{D}^{\tau_{u_x}\, s_{u_x}}_{u_x\, u_x} =& - C_{11}\, J^{\tau_{u_x} s_{u_x}} \left(\frac{\partial}{\partial x}\right)_{s_{u_x}} \left(\frac{\partial}{\partial x}\right)_{\tau_{u_x}} - C_{66}\, J^{k\tau_{u_x} s_{u_x}} \left(\frac{\partial}{\partial y}\right)_{s_{u_x}} \left(\frac{\partial}{\partial y}\right)_{\tau_{u_x}} + C_{55}\, J^{\tau_{u_{x_z}}\, s_{u_{x_z}}} \\
& - C_{16}\, J^{\tau_{u_x} s_{u_x}} \left(\frac{\partial}{\partial x}\right)_{\tau_{u_x}} \left(\frac{\partial}{\partial y}\right)_{s_{u_x}} - C_{16}\, J^{\tau_{u_x} s_{u_x}} \left(\frac{\partial}{\partial x}\right)_{s_{u_x}} \left(\frac{\partial}{\partial y}\right)_{\tau_{u_x}} \\
\\
\mathcal{D}^{\tau_{u_x}\, s_{u_y}}_{u_x\, u_y} =& - C_{12}\, J^{\tau_{u_x} s_{u_y}} \left(\frac{\partial}{\partial x}\right)_{\tau_{u_x}} \left(\frac{\partial}{\partial y}\right)_{s_{u_y}} - C_{66}\, J^{\tau_{u_x} s_{u_y}} \left(\frac{\partial}{\partial x}\right)_{s_{u_y}} \left(\frac{\partial}{\partial y}\right)_{\tau_{u_x}} \\
& - C_{16}\, J^{\tau_{u_x} s_{u_y}} \left(\frac{\partial}{\partial x}\right)_{s_{u_x}} \left(\frac{\partial}{\partial x}\right)_{\tau_{u_y}} - C_{26}\, J^{\tau_{u_x} s_{u_y}} \left(\frac{\partial}{\partial y}\right)_{s_{u_y}} \left(\frac{\partial}{\partial y}\right)_{\tau_{u_x}} z \\
\\
\mathcal{D}^{\tau_{u_x}\, s_{u_z}}_{u_x\, u_z} =& - C_{13}\, J^{k\tau_{u_x} s_{u_{z_z}}} \left(\frac{\partial}{\partial x}\right)_{\tau_{u_x}} + C_{55}\, J^{\tau_{u_{x_z}}\, s_{u_z}} \left(\frac{\partial}{\partial x}\right)_{s_{u_z}} - C_{36}\, J^{k\tau_{u_x} s_{u_z}} \left(\frac{\partial}{\partial y}\right)_{\tau_{u_x}} \\
& + C_{45}\, J^{\tau_{u_{x_z}}\, s_{u_z}} \left(\frac{\partial}{\partial y}\right)_{s_{u_z}} \\
\\
\mathcal{D}^{\tau_{u_y}\, s_{u_x}}_{u_y\, u_x} =& - C_{12}\, J^{\tau_{u_y} s_{u_x}} \left(\frac{\partial}{\partial x}\right)_{s_{u_x}} \left(\frac{\partial}{\partial y}\right)_{\tau_{u_y}} - C_{66}\, J^{\tau_{u_y} s_{u_x}} \left(\frac{\partial}{\partial x}\right)_{\tau_{u_y}} \left(\frac{\partial}{\partial y}\right)_{s_{u_x}} \\
& - C_{16}\, J^{\tau_{u_y} s_{u_x}} \left(\frac{\partial}{\partial x}\right)_{s_{u_x}} \left(\frac{\partial}{\partial x}\right)_{\tau_{u_y}} - C_{26}\, J^{\tau_{u_y} s_{u_x}} \left(\frac{\partial}{\partial y}\right)_{s_{u_x}} \left(\frac{\partial}{\partial y}\right)_{\tau_{u_y}} \\
\\
\mathcal{D}^{\tau_{u_y}\, s_{u_y}}_{u_y\, u_y} =& - C_{22}\, J^{\tau_{u_y} s_{u_y}} \left(\frac{\partial}{\partial x}\right)_{s_{u_y}} \left(\frac{\partial}{\partial x}\right)_{\tau_{u_y}} - C_{66}\, J^{\tau_{u_y} s_{u_y}} \left(\frac{\partial}{\partial x}\right)_{s_{u_x}} \left(\frac{\partial}{\partial y}\right)_{\tau_{u_y}} + C_{44}\, J^{\tau_{u_{yz}}\, s_{u_{yz}}} \\
& - C_{26}\, J^{\tau_{u_y} s_{u_y}} \left(\frac{\partial}{\partial x}\right)_{s_{u_y}} \left(\frac{\partial}{\partial y}\right)_{\tau_{u_y}} - C_{26}\, J^{\tau_{u_y} s_{u_y}} \left(\frac{\partial}{\partial x}\right)_{\tau_{u_y}} \left(\frac{\partial}{\partial y}\right)_{s_{u_y}} \\
\\
\mathcal{D}^{\tau_{u_y}\, s_{u_z}}_{u_y\, u_z} =& - C_{23}\, J^{\tau_{u_y} s_{u_{z_z}}} \left(\frac{\partial}{\partial y}\right)_{\tau_{u_y}} + C_{44}\, J^{\tau_{u_{yz}}\, s_{u_z}} \left(\frac{\partial}{\partial y}\right)_{s_{u_z}} - C_{36}\, J^{\tau_{u_y} s_{u_z}} \left(\frac{\partial}{\partial x}\right)_{\tau_{u_x}} \\
& + C_{45}\, J^{\tau_{u_{yz}}\, s_{u_z}} \left(\frac{\partial}{\partial x}\right)_{s_{u_z}} \\
\\
\mathcal{D}^{\tau_{u_z}\, s_{u_x}}_{u_z\, u_x} =& - C_{55}\, J^{\tau_{u_z} s_{u_{xz}}} \left(\frac{\partial}{\partial x}\right)_{\tau_{u_z}} + C_{13}\, J^{\tau_{u_{zz}}\, s_{u_x}} \left(\frac{\partial}{\partial x}\right)_{s_{u_x}} + C_{36}\, J^{\tau_{u_{zz}}\, s_{u_{xz}}} \left(\frac{\partial}{\partial y}\right)_{s_{u_x}} \\
& - C_{45}\, J^{\tau_{u_z} s_{u_{xz}}} \left(\frac{\partial}{\partial y}\right)_{\tau_{u_z}}
\end{aligned} \tag{22}$$

$$\mathcal{D}_{u_z\,u_y}^{\tau_{u_z}\,s_{uy}} = -\,C_{44}\,J^{\tau_{u_z}\,s_{uy_z}}\left(\frac{\partial}{\partial y}\right)_{\tau_{u_z}} + C_{23}\,J^{\tau_{uz_z}\,s_{uy}}\left(\frac{\partial}{\partial y}\right)_{s_{uy}} + C_{36}\,J^{\tau_{uz_z}\,s_{uy}}\left(\frac{\partial}{\partial x}\right)_{s_{uy}} - C_{45}\,J^{\tau_{u_z}\,s_{uy_z}}\left(\frac{\partial}{\partial x}\right)_{\tau_{u_z}}$$

$$\mathcal{D}_{u_z\,u_z}^{\tau_{u_z}\,s_{uz}} = -\,C_{44}\,J^{\tau_{u_z}\,s_{u_z}}\left(\frac{\partial}{\partial y}\right)_{s_{u_z}}\left(\frac{\partial}{\partial y}\right)_{\tau_{u_z}} - C_{55}\,J^{\tau_{u_z}\,s_{u_z}}\left(\frac{\partial}{\partial x}\right)_{s_{u_z}}\left(\frac{\partial}{\partial x}\right)_{\tau_{u_z}} + C_{33}\,J^{\tau_{u_{z_z}}\,s_{u_{z_z}}} - C_{45}\,J^{\tau_{u_z}\,s_{u_z}}\left(\frac{\partial}{\partial x}\right)_{s_{u_z}}\left(\frac{\partial}{\partial y}\right)_{\tau_{u_z}} - C_{45}\,J^{\tau_{u_z}\,s_{u_z}}\left(\frac{\partial}{\partial x}\right)_{\tau_{u_z}}\left(\frac{\partial}{\partial y}\right)_{s_{u_z}}$$

The three non-zero components of the fundamental primary differential initial stress nucleus $\mathbf{S}^{\tau s}$ are following reported

$$\mathcal{S}_{u_x\,u_x}^{\tau_{u_x}\,s_{u_x}} = J^{\tau_{u_x}\,s_{u_x}}\left[\sigma_{xx_0}^{\vartheta}\left(\frac{\partial}{\partial x}\right)_{s_{u_x}}\left(\frac{\partial}{\partial x}\right)_{\tau_{u_x}} + \sigma_{yy_0}^{\vartheta}\left(\frac{\partial}{\partial y}\right)_{s_{u_x}}\left(\frac{\partial}{\partial y}\right)_{\tau_{u_x}} + \tau_{xy_0}^{\vartheta}\left(\frac{\partial}{\partial y}\right)_{s_{u_x}}\left(\frac{\partial}{\partial x}\right)_{\tau_{u_x}}\right]$$

$$\mathcal{S}_{u_y\,u_y}^{\tau_{u_y}\,s_{u_y}} = J^{\tau_{u_y}\,s_{u_y}}\left[\sigma_{xx_0}^{\vartheta}\left(\frac{\partial}{\partial x}\right)_{s_{u_y}}\left(\frac{\partial}{\partial x}\right)_{\tau_{u_y}} + \sigma_{yy_0}^{\vartheta}\left(\frac{\partial}{\partial y}\right)_{s_{u_y}}\left(\frac{\partial}{\partial y}\right)_{\tau_{u_y}} + \tau_{xy_0}^{\vartheta}\left(\frac{\partial}{\partial y}\right)_{s_{u_y}}\left(\frac{\partial}{\partial x}\right)_{\tau_{u_y}}\right] \tag{23}$$

$$\mathcal{S}_{u_z\,u_z}^{\tau_{u_z}\,s_{u_z}} = J^{\tau_{u_z}\,s_{u_z}}\left[\sigma_{xx_0}^{\vartheta}\left(\frac{\partial}{\partial x}\right)_{s_{u_z}}\left(\frac{\partial}{\partial x}\right)_{\tau_{u_z}} + \sigma_{yy_0}^{\vartheta}\left(\frac{\partial}{\partial y}\right)_{s_{u_z}}\left(\frac{\partial}{\partial y}\right)_{\tau_{u_z}} + \tau_{xy_0}^{\vartheta}\left(\frac{\partial}{\partial y}\right)_{s_{u_z}}\left(\frac{\partial}{\partial x}\right)_{\tau_{u_z}}\right]$$

The three non-zero components of the fundamental primary mass nucleus $\mathbf{M}^{\tau s}$ are given as follows

$$\mathcal{M}_{u_x\,u_x}^{\tau_{u_x}\,s_{u_x}} = \rho\,J^{\tau_{u_x}\,s_{u_x}}$$

$$\mathcal{M}_{u_y\,u_y}^{\tau_{u_y}\,s_{u_y}} = \rho\,J^{\tau_{u_y}\,s_{u_y}} \tag{24}$$

$$\mathcal{M}_{u_z\,u_z}^{\tau_{u_z}\,s_{u_z}} = \rho\,J^{\tau_{u_z}\,s_{u_z}}$$

The three non-zero components of the fundamental primary differential boundary nucleus $\mathbf{\Sigma}^{\tau s}$, related to the initial stresses can be written as:

$$\Sigma_{u_x\,u_x}^{\tau_{u_x}\,s_{u_x}} = \sigma_{xx_0}^{\vartheta}\, J^{\tau_{u_x} s_{u_x}}\, n_x \left(\frac{\partial}{\partial x}\right)_{s_{u_x}} + \sigma_{yy_0}^{\vartheta}\, J^{\tau_{u_x} s_{u_x}}\, n_x \left(\frac{\partial}{\partial y}\right)_{s_{u_x}} + \tau_{xy_0}^{\vartheta}\, J^{\tau_{u_x} s_{u_x}}\, n_y \left(\frac{\partial}{\partial x}\right)_{s_{u_x}}$$

$$\Sigma_{u_y\,u_y}^{\tau_{u_y}\,s_{u_y}} = \sigma_{xx_0}^{\vartheta}\, J^{\tau_{u_y} s_{u_y}}\, n_x \left(\frac{\partial}{\partial x}\right)_{s_{u_y}} + \sigma_{yy_0}^{\vartheta}\, J^{\tau_{u_y} s_{u_y}}\, n_x \left(\frac{\partial}{\partial y}\right)_{s_{u_y}} + \tau_{xy_0}^{\vartheta}\, J^{\tau_{u_y} s_{u_y}}\, n_y \left(\frac{\partial}{\partial x}\right)_{s_{u_y}}$$

$$\Sigma_{u_z\,u_z}^{\tau_{u_z}\,s_{u_z}} = \sigma_{xx_0}^{\vartheta}\, J^{\tau_{u_z} s_{u_z}}\, n_x \left(\frac{\partial}{\partial x}\right)_{s_{u_z}} + \sigma_{yy_0}^{\vartheta}\, J^{\tau_{u_z} s_{u_z}}\, n_x \left(\frac{\partial}{\partial y}\right)_{s_{u_z}} + \tau_{xy_0}^{\vartheta}\, J^{\tau_{u_z} s_{u_z}}\, n_y \left(\frac{\partial}{\partial x}\right)_{s_{u_z}} \tag{25}$$

Similarly, the nine components of the primary fundamental differential boundary nucleus $\mathbf{\Pi}^{\tau s}$ can be written as:

$$\begin{aligned}\Pi_{u_x\,u_x}^{\tau_{u_x}\,s_{u_x}} &= n_x\, C_{11}\, J^{\tau_{u_x} s_{u_x}} \left(\frac{\partial}{\partial x}\right)_{s_{u_x}} + n_y\, C_{66}\, J^{\tau_{u_x} s_{u_x}} \left(\frac{\partial}{\partial y}\right)_{s_{u_x}} + n_y\, C_{16}\, J^{\tau_{u_x} s_{u_x}} \left(\frac{\partial}{\partial x}\right)_{s_{u_x}} \\ &\quad + n_x\, C_{16}\, J^{\tau_{u_x} s_{u_x}} \left(\frac{\partial}{\partial y}\right)_{s_{u_x}}\end{aligned}$$

$$\begin{aligned}\Pi_{u_x\,u_y}^{\tau_{u_x}\,s_{u_y}} &= n_y\, C_{66}\, J^{\tau_{u_x} s_{u_y}} \left(\frac{\partial}{\partial x}\right)_{s_{u_y}} + n_x\, C_{12}\, J^{\tau_{u_x} s_{u_y}} \left(\frac{\partial}{\partial y}\right)_{s_{u_y}} + n_x\, C_{16}\, J^{\tau_{u_x} s_{u_y}} \left(\frac{\partial}{\partial x}\right)_{s_{u_y}} \\ &\quad + n_y\, C_{26}\, J^{\tau_{u_x} s_{u_y}} \left(\frac{\partial}{\partial y}\right)_{s_{u_y}}\end{aligned}$$

$$\Pi_{u_x\,u_z}^{\tau_{u_x}\,s_{u_z}} = n_x\, C_{13}\, J^{\tau_{u_x} s_{u_{zz}}} + n_y\, C_{36}\, J^{\tau_{u_x} s_{u_{zz}}} \tag{26}$$

$$\begin{aligned}\Pi_{u_y\,u_x}^{\tau_{u_y}\,s_{u_x}} &= n_y\, C_{12}\, J^{\tau_{u_y} s_{u_x}} \left(\frac{\partial}{\partial x}\right)_{s_{u_x}} + n_x\, C_{66}\, J^{\tau_{u_y} s_{u_x}} \left(\frac{\partial}{\partial y}\right)_{s_{u_x}} + n_x\, C_{16}\, J^{\tau_{u_y} s_{u_x}} \left(\frac{\partial}{\partial x}\right)_{s_{u_x}} \\ &\quad + n_y\, C_{26}\, J^{\tau_{u_y} s_{u_x}} \left(\frac{\partial}{\partial y}\right)_{s_{u_x}}\end{aligned}$$

$$\begin{aligned}\Pi_{u_y\,u_y}^{\tau_{u_y}\,s_{u_y}} &= n_x\, C_{66}\, J^{\tau_{u_y} s_{u_y}} \left(\frac{\partial}{\partial x}\right)_{s_{u_y}} + n_y\, C_{22}\, J^{\tau_{u_y} s_{u_y}} \left(\frac{\partial}{\partial y}\right)_{s_{u_y}} + n_y\, C_{26}\, J^{\tau_{u_y} s_{u_y}} \left(\frac{\partial}{\partial x}\right)_{s_{u_y}} \\ &\quad + n_x\, C_{26}\, J^{\tau_{u_y} s_{u_y}} \left(\frac{\partial}{\partial y}\right)_{s_{u_y}}\end{aligned}$$

$$\Pi_{u_y\,u_z}^{\tau_{uy}\,s_{uz}} = n_y\,C_{23}\,J^{\tau_{uy}s_{uz_z}} + n_x\,C_{36}\,J^{\tau_{uy}s_{uzz}}$$

$$\Pi_{u_z\,u_x}^{\tau_{uz}\,s_{ux}} = n_x\,C_{55}\,J^{\tau_{ux}s_{ux_z}} + n_y\,C_{45}\,J^{\tau_{uz}s_{ux_z}}$$

$$\Pi_{u_z\,u_y}^{\tau_{uz}\,s_{uy}} = n_y\,C_{44}\,J^{\tau_{uz}s_{uy}} + n_x\,C_{45}\,J^{\tau_{ux}s_{uy_z}}$$

$$\Pi_{u_z\,u_z}^{\tau_{uz}\,s_{uz}} = n_x\,C_{55}\,J^{\tau_{uz}s_{uz}}\left(\frac{\partial}{\partial x}\right)_{s_{uz}} + n_y\,C_{44}\,J^{\tau_{uz}s_{uz}}\left(\frac{\partial}{\partial y}\right)_{s_{uz}} + n_y\,C_{45}\,J^{\tau_{uz}s_{uz}}\left(\frac{\partial}{\partial x}\right)_{s_{uz}} + n_x\,C_{45}\,J^{\tau_{uz}s_{uz}}\left(\frac{\partial}{\partial y}\right)_{s_{uz}}$$

The thickness integrals introduced in the fundamental nuclei are explicitly given as follows

$$J^{\tau s} = \int_A F_\tau\,F_s\,\mathrm{d}z,\quad J^{\tau_z s} = \int_A \frac{\partial F_\tau}{\partial z}\,F_s\,\mathrm{d}z,\quad J^{\tau s_z} = \int_A F_\tau\,\frac{\partial F_s}{\partial z}\,\mathrm{d}z,\quad J^{\tau_z s_z} = \int_A \frac{\partial F_\tau}{\partial z}\,\frac{\partial F_s}{\partial z}\,\mathrm{d}z \tag{27}$$

Finally, in their compact form the Eqs. (20) and (21) can be wirtten as

$$\begin{aligned} &\delta\mathbf{u}^\tau: \quad \mathbf{D}^{\tau s}\,\mathbf{u}^s + \mathbf{M}^{\tau s}\,\ddot{\mathbf{u}}^s = \mathbf{S}^{\tau s}\,\mathbf{u}^s \\ &\delta\mathbf{u}^\tau: \quad (\mathbf{\Pi}^{\tau s} - \mathbf{\Sigma}^{\tau s})\,\mathbf{u}^s = (\mathbf{\Pi}^{\tau s} - \mathbf{\Sigma}^{\tau s})\,\bar{\mathbf{u}}^s \ \text{ on } \ \Gamma_m; \quad \mathbf{u}^s = \bar{\mathbf{u}}^s \ \text{ on } \ \Gamma_g \end{aligned} \tag{28}$$

Equation (20) allows us to carry out several thermoelastic vibration analysis of the GPLRC plates under investigation by simply considering the solution of various eigenvalue problems.

6. Numerical results and discussion

The results have been computed by using the Navier-type closed form solution, and accordingly, the displacement components are expanded in double Fourier's series as follows

$$\begin{aligned} u_{x\tau_{u_x}}(x,y,t) &= \sum_m\sum_n U_{x\tau_{u_x}mn}\,\cos\left(\frac{m\,\pi\,x}{a}\right)\,\sin\left(\frac{n\,\pi\,y}{b}\right)\,e^{\imath\,\omega_{mn}\,t} \\ u_{y\tau_{u_y}}(x,y,t) &= \sum_m\sum_n U_{y\tau_{u_y}mn}\,\sin\left(\frac{m\,\pi\,x}{a}\right)\,\cos\left(\frac{n\,\pi\,y}{b}\right)\,e^{\imath\,\omega_{mn}\,t} \\ u_{z\tau_{u_z}}(x,y,t) &= \sum_m\sum_n U_{z\tau_{u_z}mn}\,\sin\left(\frac{m\,\pi\,x}{a}\right)\,\sin\left(\frac{n\,\pi\,y}{b}\right)\,e^{\imath\,\omega_{mn}\,t} \end{aligned} \tag{29}$$

where $\imath = \sqrt{-1}$, t is the time, ω_{mn} the circular frequencies associated to the half-wave numbers m and n, and $U_{x\tau_{u_x}mn}$, $U_{y\tau_{u_y}mn}$, $U_{z\tau_{u_z}mn}$ are the unknown coefficients. This solution technique implies: simply-supported boundary condition and cross-ply lamination schemes. Accorting to what just mentioned in Eqs.(22) to (26), the elastic coefficients $C_{16} = C_{26} = C_{36} = C_{45} = 0$.

The results are given using the acronyms system proposed in Refs. [47, 48]. More specifically, the acronym $ED_{N_{ux}N_{uy}N_{uz}}$ has been employed, where E means that the classical equivalent single layer approach, for the plate kinematic description, has been introduced; D states that the Principle of Virtual Displacements (PVD) (or Hamilton's principle, in the dynamic case) has been used in the analysis, and finally the three subscripts, N_{ux}, N_{uy} and N_{uz} are the expansion orders and represent independent free input parameters. The results are given in terms of dimensionless frequency and critical buckling parameters and for both, the average and maximum differences with respect those available in the literature are proposed. More specifically, the latter have been computed according to the following expressions

$$\begin{aligned} \hat{\omega} &= \omega \frac{a^2}{h}\sqrt{\frac{\rho_m}{E_m}}; \quad \Delta_\omega\% = \left(\frac{\left\|\hat{\omega}_l^i - \hat{\omega}_p^i\right\|}{\left\|\hat{\omega}_p^i\right\|}\right) \times 100; \\ \lambda_{cr} &= \sigma_{cr}\frac{b^2}{h^2 E_0}; \quad \Delta_\lambda\% = \left(\frac{\left\|\lambda_{cr_l}^i - \lambda_{cr_p}^i\right\|}{\left\|\lambda_{cr_p}^i\right\|}\right) \times 100; \end{aligned} \tag{30}$$

where the subscript p and l represent the results computed by using the present (p) formulation and those available in the literature (l), respectively.

Two different types of functionally graded (FG) distributions, of the graphene nanoplatelet reinforcements, are considered: FG-X; and FG-O. The graded distributions are carried out by using ten plies (see Ref. [22, 23]) as follows

- UD: $[0.07/0.07/0.07/0.07/0.07]_s$
- FG-X: $[0.11/0.09/0.07/0.05/0.03]_s$
- FG-O: $[0.03/0.05/0.07/0.09/0.11]_s$

As can be noted above, in the case of uniform distribution the graphene volume fraction $\mathcal{V}_G$ is considered to be 0.07 in all of the plies within the stacking sequences.

6.1. Free Vibration of FG-GPLRC Plates in Thermal environment

The first part of the results section is focused on the free vibration analyses of FG-GPLRC plates in thermal environment. More specifically, three different staking sequences: $[0]_{10}$, $[0/90/0/90/0]_s$ and $[0/90]_{5T}$, are considered. The first six dimensionless frequency parameters are computed for different GPLs patter distributions and different environmental temperatures. In Tables 3, 4 and 5 the stacking sequence $[0]_{10}$ is examined for the UD, FG-O and FG-X GPLRC plate configurations and temperature $T = 300\,K$. The results

are compared with those proposed in Ref. [23] and obtained by using the third order shear deformation theory combined with the two-step perturbation theory. An excellent agrement is found and the average and maximum difference, computed over the first six frequencies, is well below the 0.5% in the case of UD and FG-O, a slightly higher difference is found in the case of FG-X, but still below the 2.0%. Similar considerations can be drawn for the analyses carried out at temperature $T = 400\,K$. In the case-study, $T = 500\,K$ a slightly higher difference is visible in the cases of UD (below the 1%) and FG-O (below the 2%) configurations while in the FG-X (around the 1%) case it reduces. Equivalent conclusions can be inferred by observing the results Tables 6, 7 and 8 related to the stacking sequence $[0/90/0/90/0]_s$; and the results Tables 9, 10 and 11 where the stacking sequence $[0/90]_{5T}$ is analysed. In all of the case-studies addressed, as expected, an increase in the environmental temperature generated a significant reduction of the dimensionless fundamental frequency parameter.

6.2. Elastic Stability of FG-GPLRC Plates in Thermal environment

The second part of the results section is devoted to elastic buckling analysis of FG-GPLRC plates in thermal environment. The analysis has been carried out for the lamination scheme $[0/90/0/90/0]_s$ and has been restricted to the symmetric GPLRC plate configurations: UD, FG-O and FG-X. Three different thermal environments have been considered: $T = 300\,K$, $T = 400\,K$ and $T = 500\,K$. Results, related to these latter cases, are given in terms of dimensionless critical buckling loads and are shown in Tables 12, 13 and 14, respectively. Validation and assessment of the formulation are carried out by comparing the results against those proposed in Ref. [23]. As expected the $\Delta_\lambda\%$ decrease when increasing the length-to-thickness ratio. For an environmental temperature $T = 300\,K$, the lower value of $\Delta_\lambda\% = 0.05$ is obtained in the case of FG-O and $b/h = 50$, while the higher $\Delta_\lambda\% = 2.53$ in the case of FG-X and $b/h = 10$. Similarly, in the case-studies $T = 400\,K$ and $T = 500\,K$, the lower vale of $\Delta_\lambda\%$ does not change while the higher is subjected to a reduction: $\Delta_\lambda\% = 1.76$ and $\Delta_\lambda\% = 1.42$, respectively. Also, the dimensionless critical buckling load decreases while increasing the temperature. The model kinematics plays a fundamental role in the description of three dimensional local effects. In particular, the maximum benefit of the higher order model is observed when dealing with the FG-X distribution patter.

7. Conclusions

The present article investigated the elastic buckling and free vibration characteristics of temperature-dependent graphene nanoplatelet-reinforced composite (GPLRC) plates. The latter have been considered made up of three different types of reinforcements. In particular, uniformly distributed (UD) and piece-wise functionally graded: FG-O and FG-X. The effective material properties have been derived by usign various micro-mechanical models and their validity has been assessed by comparison with results available in literature and obtained by using the molecular dynamic (MD)simulations. In particular, the Young's moduli and the shear moduli have been computed by using the extended Halpin-Tsai model, the thermal expansion coefficients have been obtained by relying on the Schapery model and finally both density and Poisson's coefficients have been calculated by using the classical Voigt's rule of mixture.

The governing differential equations (GDEs) have been derived by using Hamilton's principle (HP) in conjunction with hierarchical plate models and the Gauss theorem. They have, then, been solved by using the Navier-type closed-form solution.

The investigation has unequivocally shown that the use of higher order models is a compulsory requirement when modelling the mechanical behaviour, in terms of both vibration and stability, of graphene nanoplatelet-reinforced polymer composite plates. In this respect, a significant enhancement is observed in the analysis of the FG-GPLRC plate with distribution patter FG-X, where with respect to the third order shear deformation theory (TSDT) the maximum $\Delta_\omega\%$ is obtained. Lower order plate models have not been taken into account because of their inaccuracy. The hierarchical modelling proved to be a unique computational tool, which allows analysts to capture 3D thermo-mechanical effects in composite structures reinforced by carbonaceous nano-fillers. The analysis has also shown the effect of the thermal environment on both the dimensionless frequency parameters and the dimensionless critical buckling loads. In this respect, a significant decrease of these latter has been observed in the temperature range considered in this investigation.

References

[1] K. S. Novoselov, A. K. Geim, S. V. Morozov, D. Jiang, Y. Zhang, S. V. Dubonos, I. V. Grigorieva, F. A. A., Electric field effect in atomically thin carbon films, Science 306 (5696) (2004) 666–669.

[2] M. Kaseem, K. Hamad, Y. G. Ko, Fabrication and materials properties of polystyrene/carbon nanotube (PS/CNT) composites: a review, Eur Polymer J 79 (2016) 36–72.

[3] Z. Spitalsky, D. Tasis, K. Papagelis, C. Galiotis, Carbon nanotubepolymer composites: chemistry, processing, mechanical and electrical properties, Prog Polym Sci 35 (2010) 357–401.

[4] M. A. Rafiee, J. Rafiee, Z. Wang, H. Song, Z. Z. Yu, N. Koratkar, Enhanced mechanical properties of nanocomposites at low graphene content, ACS Nano 3 (2009) 3884–3890.

[5] J. Liang, Y. Huang, L. Zhang, Y. Wang, Y. Ma, T. Guo, Y. Chen, Molecular-level dispersion of graphene into poly(vinyl alcohol) and effective reinforcement of their nanocomposites, Advanced Functional Materials 19 (2009) 2297–2302.

[6] X. Zhao, Y. Y. Lee, K. M. Liew, Mechanical and thermal buckling analysis of functionally graded plates, Composite Structures 90 (2) (2009) 161–171.

[7] F. Wang, L. T. Drzal, Y. Qin, Z. Huang, Mechanical properties and thermal conductivity of graphene nanoplatelet/epoxy composites, Composite Structures 50 (3) (2015) 1082–1093.

[8] M. Fang, K. Wang, H. Lu, Y. Yang, S. Nutt, Covalent polymer functionalization of graphene nanosheets and mechanical properties of composites, Journal of Materials Chemistry 19 (2009) 7098–7105.

[9] K. N. Spanos, S. K. Georgantzinos, N. K. Anifantis, Investigation of stress transfer in carbon nanotube reinforced composites using a multi-scale finite element approach, Compos. Part B: Eng. 63 (2014) 85–93.

[10] F. Lin, H.-S. Shen, Temperature dependent mechanical properties of graphene reinforced polymer nanocomposites e a molecular dynamics simulation, Composites Part B: Eng 11 (2017) 261–269.

[11] H. Khezerlou, M. Tahmasebipour, Molecular dynamic simulation of graphenepoly methyl methacrylate nano-composite, J Nanoelectron Optoelectron 9 (2014) 580–583.

[12] R. E. Roussou, K. Karatasos, Graphene/poly(ethylene glycol) nanocomposites as studied by molecular dynamics simulations, Mater Des 97 (2016) 163–174.

[13] R. Rahman, A. Haque, Molecular modeling of crosslinked grapheneeepoxy nanocomposites for characterization of elastic constants and interfacial properties, Compos part B: Eng 54 (2013) 353–364.

[14] Y. Zhang, X. Zhuang, J. Muthu, T. Mabrouki, M. Fontaine, Y. Gong, T. Timon Rabczuk, Load transfer of graphene/carbon nanotube/polyethylene hybrid nanocomposite by molecular dynamics simulation, Compos B-Eng 63 (2014) 27–33.

[15] A. N. Rissanou, V. Harmandaris, Structure and dynamics of poly(- methylmethacrylate)/graphene systems through atomistic molecular dynamics simulations, J Nanoparticle Res 15 (1589) (2013) 1–14.

[16] F. Liu, N. Hu, H. Ning, Y. Liu, Y. Li, L. Wu, Molecular dynamics simulation on interfacial mechanical properties of polymer nanocomposites with wrinkled graphene, Composites Part B: Eng 108 (2015) 160–167.

[17] R. Ansari, S. Ajori, B. Motevalli, Mechanical properties of defective singlelayered graphene sheets via molecular dynamics simulation, Superlattices Microstruct 51 (2012) 274–289.

[18] E. Garcia-Macias, L. Garcia-Macas, A. Saez, Bending and free vibration analysis of functionally graded graphene vs. carbon nanotube reinforced composite plates, Composite Structures 186 (2018) 123–138.

[19] M. Song, J. Yang, S. Kitipornchai, Bending and buckling analyses of functionally graded polymer composite plates reinforced with graphene nanoplatelets, Compos. Part B: Eng. 134 (2018) 106–113.

[20] M. Mirzaei, Y. Kiani, Isogeometric thermal buckling analysis of temperature dependent fg graphene reinforced laminated plates using nurbs formulation, Composite Structures (2017) 606–616.

[21] R. Gholami, R. Ansari, Nonlinear harmonically excited vibration of third-order shear deformable functionally graded graphene platelet-reinforced composite rectangular plates, Engineering Structures 156 (2018) 197–209.

[22] Y. Kiani, Isogeometric large amplitude free vibration of graphene reinforced laminated plates in thermal environment using nurbs formulation, Comput. Methods Appl. Mech. Engrg 332 (2018) 86–101.

[23] H.-S. Shen, Y. Xiang, F. Lin, Nonlinear vibration of functionally graded graphene-reinforced composite laminated plates in thermal environments, Comput. Methods Appl. Mech. Engrg 319 (2017) 175–193.

[24] M. Song, S. Kitipornchai, J. Yang, Free and forced vibrations of functionally graded polymer composite plates reinforced with graphene nanoplatelets, Composite Structures 159 (2017) 579–588.

[25] S. M. Hosseini, C. Zhang, Coupled thermoelastic analysis of an fg multilayer graphene platelets-reinforced nanocomposite cylinder using meshless gfd method: A modified micromechanical model, Engineering Analysis with Boundary Elements 88 (2018) 80–92.

[26] F. A. Fazzolari, Quasi-3D beam models for the computation of eigenfrequencies of functionally graded beams with arbitrary boundary conditions, Composite Structures 154 (2016) 239–255.

[27] F. A. Fazzolari, Generalized exponential, polynomial and trigonometric theories for vibration and stability analysis of porous fg sandwich beams resting on elastic foundations, Composites Part B: Engineering 136 (2018) 254–271.

[28] F. A. Fazzolari, Reissner's mixed variational theorem and variable kinematics in the modelling of laminated composite and FGM doubly-curved shells, Composites Part B: Engineering 89 (2016) 408–423.

[29] F. A. Fazzolari, Natural frequencies and critical temperatures of functionally graded sandwich plates subjected to uniform and non-uniform temperature distributions, Composite Structures 121 (2015) 197–210.

[30] F. A. Fazzolari, Thermoelastic vibration and stability of temperature-dependent carbon nanotube-reinforced composite plates, Composite Structures 196 (2018) 199–214.

[31] F. A. Fazzolari, Modal characteristics of P-and S-FGM plates with temperature-dependent materials in thermal environment, Journal of Thermal Stresses 39 (7) (2016) 854–873.

[32] F. A. Fazzolari, J. R. Banerjee, Axiomatic/asymptotic PVD/RMVT-based shell theories for free vibrations of anisotropic shells using an advanced Ritz formulation and accurate curvature descriptions, Composite Structures 108 (2014) 91–110.

[33] F. A. Fazzolari, Stability analysis of FGM sandwich plates by using variable-kinematics Ritz models, Mechanics of Advanced Materials and Structures 23 (4) (2016) 1104–1113.

[34] F. A. Fazzolari, Sandwich Structures, Elsevier, Woodhead Publishing, 2017, Ch. 2, pp. 49–90.

[35] R. A. Schapery, Thermal expansion coefficient of composite materials based on energy principles, Journal of Composite Materials 2 (1968) 380–404.

[36] J. N. Reddy, Mechanics of laminated composite plates and shells. Theory and Analysis, 2nd Edition, CRC Press, 2004.

[37] R. M. Jones, Mechanics of composite materials, 2nd Edition, Taylor & Francis, United States, 1998.

[38] G. R. Kirchhoff, Über das Gleichgewicht und die Bewegung einer elastischen Sheibe. (About the equilibrium and motion of elastic bodies.), Journal für die Reine und Angewandte Mathematik 40 (1850) 51–88.

[39] A. E. H. Love, A treatise on the mathematical theory of elasticity, 4th Edition, Dover Pub., New York, 1944.

[40] A. E. H. Love, The small free vibrations and deformations of a thin elastic shell, Phil. Trans. Roy. Soc. (London) ser. A (179) (1888) 491–549.

[41] E. Reissner, The effect of transverse shear deformation on the bending of elastic plates., Journal of Applied Mechanics 67 (1945) A67–A77.

[42] R. Mindlin, Influence of rotary inertia and shear on flexural motions of isotropic elastic plates., Journal of Applied Mechanics 18 (10) (1951) 31–38.

[43] K. Washizu, Variational Methods in Elasticity and Plasticity, 1st Edition, Pergamon, Headington Hill Hall, Oxford, 1968.

[44] H. Matsunaga, Free vibration and stability of functionally graded plates according to a 2-d higher-order deformation theory, Composite Structures 82 (4) (2008) 499–512.

[45] E. Carrera, A class of two-dimensional theories for anisotropic multilayered plates analysis, Atti Accademia delle scienze Torino, Memorie Scienze Fisiche 19-20 (1995) 49–87.

[46] E. Carrera, Theories and finite elements for multilayered plates and shells: a unified compact formulation with numerical assessment and benchmarking, Archives of Computational Methods in Engineering 10 (3) (2003) 216–296.

[47] F. A. Fazzolari, E. Carrera, Accurate free vibration analysis of thermo-mechanically pre/post-buckled anisotropic multilayered plates based on a refined hierarchical trigonometric Ritz formulation., Composite Structures 95 (2013) 381–402.

[48] F. A. Fazzolari, E. Carrera, Coupled thermoelastic effect in free vibration analysis of anisotropic multilayered plates and fgm plates by using a variable-kinematics Ritz formulation, European Journal of Mechanics Solid/A, 44 (2014) 157–174.

[49] S. W. Tsai, Composites Design, 4th Edition, Dayton, Think Composites, 1988.

[50] Y. Han, J. Elliott, Molecular dynamics simulations of the elastic properties of polymer/carbon nanotube composites, Computational Materials Science 39 (2007) 315–323.

[51] P. Zhu, Z. X. Lei, K. M. Liew, Static and free vibration analyses of carbon nanotube-reinforced composite plates using finite element method with first order shear deformation plate theory, Composite Structures 94 (4) (2012) 1450–1460.

Appendix A

The thermo-mechanical coupling coefficients expressed in the laminate reference system are:

$$\mathbf{\Xi}\left(z,T\right)=\mathbf{C}\left(z,T\right)\,\boldsymbol{\alpha}\left(z,T\right) \tag{31}$$

where the vector including the coefficients of thermal expansion and the constitutive matrix are given in Eqs. (12) and (13), respectively. In vectorial form, they assume the following form:

$$\mathbf{\Xi}=\left[\begin{array}{cccccc}\xi_x & \xi_y & \xi_{xy} & 0 & 0 & \xi_z\end{array}\right]^T \tag{32}$$

and explicitly

$$\begin{aligned}\xi_x&=C_{11}\,\alpha_x+C_{12}\,\alpha_y+C_{16}\,\alpha_{xy}+C_{13}\,\alpha_z\\ \xi_y&=C_{12}\,\alpha_x+C_{22}\,\alpha_y+C_{26}\,\alpha_{xy}+C_{23}\,\alpha_z\\ \xi_{xy}&=C_{16}\,\alpha_x+C_{26}\,\alpha_y+C_{66}\,\alpha_{xy}+C_{36}\,\alpha_z\\ \xi_z&=C_{13}\,\alpha_x+C_{23}\,\alpha_y+C_{36}\,\alpha_{xy}+C_{33}\,\alpha_z\end{aligned} \tag{33}$$

At this stage it is useful to recall that the pre-buckling stresses and displacements satisfy the equations of equilibrium within each layer and at the interface between layers, as well as the stress free boundary conditions at the top and bottom surfaces of the plate.

The thermal stresses due to the temperature variation for an individual layer, under the plane stress assumption $\left(\sigma^{\vartheta}_{zz_0}=0,\,\varepsilon^{\vartheta}_{zz_0}\neq 0\right)$, can be defined as follows

$$\tilde{\sigma}^{\vartheta}_{xx_0}=\tilde{\xi}_x\,\Delta T_0;\quad \tilde{\sigma}^{\vartheta}_{yy_0}=\tilde{\xi}_y\,\Delta T_0;\quad \tilde{\tau}^{\vartheta}_{xy_0}=\tilde{\xi}_{xy}\,\Delta T_0 \tag{34}$$

The reduced thermo-mechanical coupling coefficients, appearing in Eq. (34), are expressed in terms of reduced elastic coefficients in the following manner

$$\begin{aligned}\tilde{\xi}_x&=\chi_{11}\,\alpha_x+\chi_{12}\,\alpha_y+\chi_{13}\,\alpha_{xy}\\ \tilde{\xi}_y&=\chi_{21}\,\alpha_x+\chi_{22}\,\alpha_y+\chi_{23}\,\alpha_{xy}\\ \tilde{\xi}_{xy}&=\chi_{31}\,\alpha_x+\chi_{32}\,\alpha_y+\chi_{33}\,\alpha_{xy}\end{aligned} \tag{35}$$

where

$$\begin{aligned}&\chi_{11}=C_{11}-\frac{C_{13}^2}{C_{33}};\quad \chi_{12}=C_{12}-\frac{C_{13}\,C_{23}}{C_{33}};\quad \chi_{13}=C_{16}-\frac{C_{13}\,C_{36}}{C_{33}};\\ &\chi_{21}=C_{12}-\frac{C_{13}\,C_{23}}{C_{33}};\quad \chi_{22}=C_{22}-\frac{C_{23}^2}{C_{33}};\quad \chi_{23}=C_{26}-\frac{C_{23}\,C_{36}}{C_{33}};\\ &\chi_{31}=C_{16}-\frac{C_{13}\,C_{36}}{C_{33}};\quad \chi_{32}=C_{26}-\frac{C_{23}\,C_{23}}{C_{33}};\quad \chi_{33}=C_{66}-\frac{C_{36}^2}{C_{33}};\end{aligned} \tag{36}$$

Through Eqs. (34) the temperature variation ΔT_0 is assigned in the model. $\tilde{\xi}_x$, $\tilde{\xi}_y$ and $\tilde{\xi}_{xy}$ are the two in-plane and the shear coefficients relating thermal stresses to temperature variation, respectively . $\xi_{xy} = 0$ in the case of cross-ply laminations. For the sake of conciseness, the dependence of the coefficients C_{ij} versus Young's moduli, Poisson's ratio, shear moduli and the fiber angle is not provided. It can be found in various textbooks such as those proposed by Tsai [49], Reddy [36] or Jones [37].

Tables

Table 1: Temperature-dependent material properties for monolayer graphene (length - $a_G = 14.76\,\text{nm}$, width - $b_G = 14.77\,\text{nm}$, thickness - $h_G = 0.188\,\text{nm}$, Poisson'ratio - $\nu_{12}^G = 0.177$, density - $\rho_G = 4118\,\text{kg/m}^3$) [].

Temperature	E_{11}^G (GPa)	E_{22}^G (GPa)	G_{12}^G (GPa)	α_{11}^G (10^{-6}/K)	α_{22}^G (10^{-6}/K)
300	1812	1807	683	−0.90	−0.95
400	1769	1763	691	−0.35	−0.40
500	1748	1735	700	−0.08	−0.08

Table 2: Comparisons of Young's and shear moduli for graphene/PMMA nanocomposites.

V_G	MD[50]			Extended HalpinTsai model					
	E_{11} (GPa)	E_{22} (GPa)	G_{12} GPa	E_{11} (GPa)	η_1	E_{22} (GPa)	η_2	G_{12} (GPa)	η_3
$T = 300\,\text{K}$									
0.03	36.538	35.613	11.388	12.47	2.929	12.47	2.855	0.962	11.842
0.05	59.544	57.479	15.655	19.41	3.068	19.41	2.962	0.982	15.944
0.07	80.096	78.843	23.644	26.58	3.013	26.58	2.966	1.003	23.575
0.09	90.023	88.750	33.635	34.01	2.647	34.01	2.609	1.025	32.816
0.11	96.388	94.265	34.713	41.71	2.311	41.71	2.260	1.048	33.125
$T = 400\,\text{K}$									
0.03	32.639	31.750	11.572	10.96	2.977	10.96	2.896	0.831	13.928
0.05	53.462	51.661	12.919	17.09	3.128	17.09	3.023	0.848	15.229
0.07	71.698	70.928	19.574	23.43	3.060	23.43	3.027	0.867	22.588
0.09	81.035	78.091	25.566	30.01	2.701	30.00	2.603	0.886	28.869
0.11	88.557	86.063	26.735	36.82	2.405	36.82	2.337	0.906	29.527
$T = 500\,\text{K}$									
0.03	31.926	31.854	11.700	9.424	3.388	9.420	3.382	0.700	16.712
0.05	52.171	50.225	11.450	14.72	3.544	14.71	3.414	0.715	16.018
0.07	69.960	67.453	17.106	20.21	3.462	20.20	3.339	0.730	23.428
0.09	79.218	76.019	22.202	25.90	3.058	25.89	2.936	0.746	29.754
0.11	87.039	84.743	23.478	31.82	2.736	31.80	2.665	0.763	30.773

Table 3: First 6 dimensionless frequency parameters of simply-supported UD and FG-GPLs reinforced composite plates with lay-out $[0]_{10}$ and $T = 300\,\mathrm{K}$.

Theory	CNTs	Dimensionless circular frequency parameters							
		$\hat{\omega}_1$	$\hat{\omega}_2$	$\hat{\omega}_3$	$\hat{\omega}_4$	$\hat{\omega}_5$	$\hat{\omega}_6$	Ave. $\Delta\%$	Max $\Delta\%$
TSPT[51]	UD	28.0982	64.8785	65.1157	95.6901	116.0301	116.4778		
ED_{999}		28.120410	64.993707	65.231631	95.933161	116.364694	116.813467	(0.21)	(0.29)
ED_{888}		28.120410	64.993707	65.231631	95.933161	116.364694	116.813467	(0.21)	(0.29)
ED_{777}		28.120410	64.993707	65.231631	95.933161	116.364694	116.813468	(0.21)	(0.29)
ED_{666}		28.120410	64.993709	65.231632	95.933169	116.364718	116.813492	(0.21)	(0.29)
ED_{555}		28.120418	64.993968	65.231901	95.934342	116.367523	116.816421	(0.21)	(0.29)
ED_{444}		28.121572	65.007602	65.245747	95.976607	116.441317	116.891476	(0.25)	(0.36)
TSPT	FG-O	23.5769	56.0228	56.3974	84.5665	103.7875	104.5809		
ED_{999}		23.584772	56.066490	56.438706	84.674282	103.925589	104.708136	(0.09)	(0.13)
ED_{888}		23.584774	56.066503	56.438716	84.674320	103.925650	104.708187	(0.09)	(0.13)
ED_{777}		23.585225	56.068551	56.440758	84.679355	103.931281	104.713795	(0.10)	(0.14)
ED_{666}		23.585226	56.068605	56.440793	84.679592	103.931931	104.714347	(0.10)	(0.14)
ED_{555}		23.590049	56.095132	56.468771	84.733040	104.017976	104.806101	(0.16)	(0.22)
ED_{444}		23.591529	56.102096	56.476057	84.750142	104.044401	104.833717	(0.17)	(0.25)
TSPT	FG-X	29.5212	65.6449	65.9070	95.6293	113.4456	113.9093		
ED_{999}		29.298236	64.756519	65.008405	94.096942	111.471543	111.918009	(1.43)	(1.75)
ED_{888}		29.298291	64.756905	65.008765	94.097866	111.473003	111.919417	(1.43)	(1.75)
ED_{777}		29.327578	64.876016	65.129794	94.308863	111.747590	112.198062	(1.23)	(1.50)
ED_{666}		29.327645	64.877234	65.130971	94.312510	111.753716	112.204091	(1.23)	(1.50)
ED_{555}		29.470215	65.456675	65.716757	95.330947	113.074752	113.535772	(0.29)	(0.33)
ED_{444}		29.471385	65.480713	65.741468	95.413017	113.215155	113.679705	(0.22)	(0.25)

Table 4: First 6 dimensionless frequency parameters of simply-supported UD and FG-GPLs reinforced composite plates with lay-out $[0]_{10}$ and $T = 400\,\mathrm{K}$.

Theory	CNTs	Dimensionless circular frequency parameters							
		$\hat{\omega}_1$	$\hat{\omega}_2$	$\hat{\omega}_3$	$\hat{\omega}_4$	$\hat{\omega}_5$	$\hat{\omega}_6$	Ave. $\Delta\%$	Max $\Delta\%$
TSPT[51]	UD	21.9591	54.8037	57.6844	84.0640	101.1662	105.3867		
ED_{999}		21.930306	54.800265	57.735233	84.180280	101.315475	105.627521	(0.12)	(0.23)
ED_{888}		21.930306	54.800265	57.735233	84.180280	101.315475	105.627521	(0.12)	(0.23)
ED_{777}		21.930306	54.800265	57.735233	84.180280	101.315475	105.627521	(0.12)	(0.23)
ED_{666}		21.930306	54.800266	57.735235	84.180290	101.315506	105.627552	(0.12)	(0.23)
ED_{555}		21.930318	54.800603	57.735564	84.181679	101.319032	105.631044	(0.12)	(0.23)
ED_{444}		21.931765	54.816383	57.750740	84.227437	101.400502	105.710296	(0.17)	(0.31)
TSPT	FG-O	17.5580	46.4214	49.6313	73.9941	89.5692	94.2338		
ED_{999}		17.514996	46.352881	49.625916	73.989772	89.558719	94.341730	(0.09)	(0.24)
ED_{888}		17.515003	46.352915	49.625933	73.989832	89.558816	94.341784	(0.09)	(0.24)
ED_{777}		17.515326	46.354047	49.627045	73.992876	89.561404	94.344441	(0.09)	(0.24)
ED_{666}		17.515336	46.354058	49.627057	73.993013	89.561769	94.344818	(0.09)	(0.24)
ED_{555}		17.520966	46.380379	49.652496	74.045836	89.640627	94.422835	(0.11)	(0.21)
ED_{444}		17.523018	46.389831	49.661810	74.067865	89.676680	94.459067	(0.13)	(0.24)
TSPT	FG-X	23.8137	56.1356	58.8911	84.4575	99.7253	103.9394		
ED_{999}		23.653977	55.616973	58.432817	83.707031	98.741804	103.059763	(0.85)	(0.99)
ED_{888}		23.654014	55.617203	58.433019	83.707545	98.742645	103.060518	(0.85)	(0.99)
ED_{777}		23.663849	55.656074	58.470628	83.772619	98.830812	103.145895	(0.78)	(0.89)
ED_{666}		23.663862	55.656666	58.471231	83.774594	98.834258	103.149301	(0.78)	(0.90)
ED_{555}		23.746185	55.973666	58.777878	84.297749	99.520772	103.813050	(0.21)	(0.29)
ED_{444}		23.747424	55.998413	58.802193	84.377235	99.661934	103.952253	(0.14)	(0.29)

Table 5: First 6 dimensionless frequency parameters of simply-supported UD and FG-GPLs reinforced composite plates with lay-out $[0]_{10}$ and $T = 500\,\mathrm{K}$.

Theory	CNTs	Dimensionless circular frequency parameters							
		$\hat{\omega}_1$	$\hat{\omega}_2$	$\hat{\omega}_3$	$\hat{\omega}_4$	$\hat{\omega}_5$	$\hat{\omega}_6$	Ave. $\Delta\%$	Max $\Delta\%$
TSPT[51]	UD	15.0773	45.2749	52.0752	74.6301	88.3236	97.9272		
ED_{999}		14.956996	45.120856	52.057768	74.610722	88.272498	98.080373	(0.24)	(0.80)
ED_{888}		14.956996	45.120856	52.057768	74.610722	88.272498	98.080373	(0.24)	(0.80)
ED_{777}		14.956996	45.120856	52.057768	74.610723	88.272499	98.080374	(0.24)	(0.80)
ED_{666}		14.956996	45.120858	52.057770	74.610736	88.272540	98.080416	(0.24)	(0.80)
ED_{555}		14.957016	45.121331	52.058220	74.612504	88.277178	98.085061	(0.23)	(0.80)
ED_{444}		14.959202	45.140659	52.075726	74.663936	88.369645	98.172188	(0.24)	(0.78)
TSPT	FG-O	9.8081	37.5828	44.6734	66.0903	78.7036	88.1220		
ED_{999}		9.622112	37.313078	44.581702	65.896912	78.400046	88.117790	(0.58)	(1.89)
ED_{888}		9.622115	37.313083	44.581702	65.896912	78.400048	88.117790	(0.58)	(1.89)
ED_{777}		9.622289	37.313479	44.581979	65.897974	78.400769	88.118265	(0.58)	(1.89)
ED_{666}		9.622289	37.313571	44.582029	65.898323	78.401625	88.118884	(0.58)	(1.89)
ED_{555}		9.635959	37.356824	44.617552	65.976204	78.518263	88.220048	(0.50)	(1.76)
ED_{444}		9.641302	37.373274	44.630753	66.007650	78.572157	88.267466	(0.46)	(1.70)
TSPT	FG-X	18.2243	48.1752	54.0462	76.4753	89.1503	97.7478		
ED_{999}		18.028835	47.719216	53.725715	75.969626	88.480745	97.275250	(0.75)	(1.07)
ED_{888}		18.028848	47.719307	53.725801	75.969843	88.481111	97.275581	(0.75)	(1.07)
ED_{777}		18.031101	47.727158	53.732760	75.981416	88.497361	97.290071	(0.74)	(1.06)
ED_{666}		18.031112	47.727655	53.733212	75.982917	88.500071	97.292527	(0.74)	(1.06)
ED_{555}		18.093667	47.937315	53.924493	76.299747	88.915119	97.676821	(0.33)	(0.72)
ED_{444}		18.095703	47.968686	53.952268	76.388699	89.077886	97.825805	(0.26)	(0.71)

Table 6: First 6 dimensionless frequency parameters of simply-supported UD and FG-GPLs reinforced composite plates with lay-out $[0/90/0/90/0]_s$ and $T = 300\,\mathrm{K}$.

Theory	CNTs	Dimensionless circular frequency parameters							
		$\hat{\omega}_1$	$\hat{\omega}_2$	$\hat{\omega}_3$	$\hat{\omega}_4$	$\hat{\omega}_5$	$\hat{\omega}_6$	Ave. $\Delta\%$	Max $\Delta\%$
TSPT[51]	UD	28.0982	64.9584	65.0364	95.6904	116.1739	116.3356		
ED_{999}		28.120437	65.074265	65.151696	95.933401	116.510591	116.669217	(0.21)	(0.29)
ED_{888}		28.120437	65.074265	65.151696	95.933401	116.510591	116.669217	(0.21)	(0.29)
ED_{777}		28.120437	65.074266	65.151697	95.933402	116.510592	116.669222	(0.21)	(0.29)
ED_{666}		28.120437	65.074266	65.151702	95.933410	116.510601	116.669267	(0.21)	(0.29)
ED_{555}		28.120445	65.074517	65.151980	95.934583	116.513370	116.672233	(0.21)	(0.29)
ED_{444}		28.121599	65.087945	65.166035	95.976847	116.586692	116.747766	(0.25)	(036)
TSPT	FG-O	23.5769	56.2111	56.2103	84.5669	104.1813	104.1911		
ED_{999}		23.584811	56.251699	56.254858	84.674711	104.318769	104.319106	(0.09)	(0.13)
ED_{888}		23.584812	56.251712	56.254868	84.674749	104.318835	104.319154	(0.09)	(0.13)
ED_{777}		23.585264	56.253884	56.256792	84.679788	104.324292	104.324962	(0.10)	(0.14)
ED_{666}		23.585265	56.253971	56.256808	84.680024	104.324694	104.325799	(0.10)	(0.14)
ED_{555}		23.590086	56.280922	56.284354	84.733466	104.413437	104.414840	(0.16)	(0.22)
ED_{444}		23.591567	56.288321	56.291208	84.750568	104.441078	104.441249	(0.17)	(0.25)
TSPT	FG-X	29.5212	65.7134	65.8394	95.6296	113.5548	113.8022		
ED_{999}		29.298289	64.818151	64.947635	94.097286	111.565280	111.826149	(1.43)	(1.75)
ED_{888}		29.298345	64.818534	64.947998	94.098210	111.566752	111.827544	(1.43)	(1.75)
ED_{777}		29.327631	64.938108	65.068567	94.309210	111.841654	112.105903	(1.23)	(1.50)
ED_{666}		29.327698	64.939365	65.069706	94.312857	111.847977	112.111739	(1.23)	(1.50)
ED_{555}		29.470266	65.522720	65.651595	95.331303	113.177531	113.435024	(0.29)	(0.33)
ED_{444}		29.471436	65.546437	65.676633	95.413371	113.317256	113.579642	(0.22)	(0.25)

Table 7: First 6 dimensionless frequency parameters of simply-supported UD and FG-GPLs reinforced composite plates with lay-out $[0/90/0/90/0]_s$ and $T = 400\,\mathrm{K}$.

Theory	CNTs	Dimensionless circular frequency parameters							
		$\hat{\omega}_1$	$\hat{\omega}_2$	$\hat{\omega}_3$	$\hat{\omega}_4$	$\hat{\omega}_5$	$\hat{\omega}_6$	Ave. $\Delta\%$	Max $\Delta\%$
TSPT[51]	UD	21.9591	55.9631	56.5605	84.0641	102.8508	103.7435		
ED_{999}		21.930322	55.980392	56.591925	84.180401	103.034887	103.951579	(0.12)	(0.20)
ED_{888}		21.930322	55.980392	56.591925	84.180401	103.034887	103.951579	(0.12)	(0.20)
ED_{777}		21.930322	55.980392	56.591926	84.180401	103.034888	103.951584	(0.12)	(0.20)
ED_{666}		21.930322	55.980393	56.591928	84.180411	103.034915	103.951619	(0.12)	(0.20)
ED_{555}		21.930334	55.980713	56.592273	84.181800	103.038341	103.955210	(0.12)	(0.20)
ED_{444}		21.931781	55.995945	56.607972	84.227558	103.117870	104.036322	(0.17)	(0.28)
TSPT	FG-O	17.5581	47.8107	48.2951	73.9946	91.5963	92.2668		
ED_{999}		17.515052	47.771256	48.262919	73.990275	91.643192	92.320986	(0.09)	(0.25)
ED_{888}		17.515059	47.771277	48.262948	73.990335	91.643253	92.321072	(0.09)	(0.25)
ED_{777}		17.515382	47.772325	48.264145	73.993381	91.645595	92.323994	(0.08)	(0.24)
ED_{666}		17.515391	47.772327	48.264174	73.993518	91.645856	92.324495	(0.08)	(0.24)
ED_{555}		17.521021	47.798214	48.289983	74.046338	91.724216	92.402923	(0.10)	(0.21)
ED_{444}		17.523073	47.807070	48.299888	74.068368	91.758798	92.440625	(0.11)	(0.20)
TSPT	FG-X	23.8138	57.2699	57.7903	84.4584	101.4343	102.2760		
ED_{999}		23.654129	56.770218	57.314861	83.707998	100.478618	101.371505	(0.85)	(0.94)
ED_{888}		23.654165	56.770469	57.315044	83.708512	100.479521	101.372204	(0.85)	(0.94)
ED_{777}		23.664000	56.808151	57.353791	83.773590	100.564266	101.460923	(0.75)	(0.86)
ED_{666}		23.664014	56.808837	57.354306	83.775565	100.568030	101.464028	(0.75)	(0.85)
ED_{555}		23.746334	57.123437	57.662959	84.298728	101.250278	102.131424	(0.21)	(0.28)
ED_{444}		23.747573	57.147130	57.688312	84.378214	101.387841	102.274135	(0.13)	(0.28)

Table 8: First 6 dimensionless frequency parameters of simply-supported UD and FG-GPLs reinforced composite plates with lay-out $[0/90/0/90/0]_s$ and $T = 500\,\mathrm{K}$.

Theory	CNTs	Dimensionless circular frequency parameters							
		$\hat{\omega}_1$	$\hat{\omega}_2$	$\hat{\omega}_3$	$\hat{\omega}_4$	$\hat{\omega}_5$	$\hat{\omega}_6$	Ave. $\Delta\%$	Max $\Delta\%$
TSPT[51]	UD	15.0776	48.0719	49.5070	74.6317	92.2023	94.2890		
ED_{999}		14.957266	47.974275	49.443329	74.612247	92.234607	94.370915	(0.21)	(0.80)
ED_{888}		14.957266	47.974275	49.443329	74.612247	92.234607	94.370915	(0.21)	(0.80)
ED_{777}		14.957267	47.974282	49.443336	74.612252	92.234626	94.370953	(0.21)	(0.80)
ED_{666}		14.957267	47.974282	49.443346	74.612265	92.234644	94.371027	(0.21)	(0.80)
ED_{555}		14.957288	47.974692	49.443856	74.614036	92.238962	94.375978	(0.21)	(0.80)
ED_{444}		14.959474	47.992218	49.462945	74.665463	92.326001	94.468001	(0.23)	(0.78)
TSPT	FG-O	9.8082	40.7210	41.8332	66.0909	82.8460	84.2405		
ED_{999}		9.622220	40.533070	41.676688	65.897483	82.673133	84.124676	(0.56)	(1.90)
ED_{888}		9.622224	40.533082	41.676689	65.897483	82.673146	84.124683	(0.56)	(1.90)
ED_{777}		9.622397	40.533410	41.677016	65.898543	82.673718	84.125268	(0.56)	(1.89)
ED_{666}		9.622398	40.533467	41.677095	65.898892	82.674412	84.126030	(0.56)	(1.89)
ED_{555}		9.636068	40.573672	41.714721	65.976774	82.786335	84.230706	(0.44)	(1.76)
ED_{444}		9.641410	40.588265	41.729373	66.008215	82.836357	84.281436	(0.41)	(1.70)
TSPT	FG-X	18.2245	50.6451	51.7409	76.4767	92.7234	94.3692		
ED_{999}		18.029107	50.240871	51.378088	75.971008	92.122373	93.839611	(0.74)	(1.07)
ED_{888}		18.029120	50.240977	51.378160	75.971226	92.122781	93.839904	(0.74)	(1.07)
ED_{777}		18.031373	50.248046	51.385827	75.982803	92.137080	93.856251	(0.73)	(1.06)
ED_{666}		18.031384	50.248600	51.386226	75.984304	92.139918	93.858579	(0.72)	(1.06)
ED_{555}		18.093935	50.450865	51.583217	76.301143	92.543779	94.251968	(0.33)	(0.72)
ED_{444}		18.095971	50.479789	51.613124	76.390086	92.697973	94.408543	(0.24)	(0.70)

Table 9: First 6 dimensionless frequency parameters of simply-supported UD and FG-GPLs reinforced composite plates with lay-out $[0/90]_{5T}$ and $T = 300\,\mathrm{K}$.

Theory	CNTs	Dimensionless circular frequency parameters							
		$\hat{\omega}_1$	$\hat{\omega}_2$	$\hat{\omega}_3$	$\hat{\omega}_4$	$\hat{\omega}_5$	$\hat{\omega}_6$	Ave. $\Delta\%$	Max $\Delta\%$
TSPT[51]	UD	28.0982	64.9974	64.9974	95.6903	116.2548	116.2548		
ED_{999}		28.120418	65.112958	65.112958	95.933354	116.589890	116.589890	(0.21)	(0.29)
ED_{888}		28.120418	65.112959	65.112959	95.933355	116.589893	116.589893	(0.21)	(0.29)
ED_{777}		28.120418	65.112959	65.112959	95.933355	116.589895	116.589895	(0.21)	(0.29)
ED_{666}		28.120418	65.112961	65.112961	95.933363	116.589921	116.589921	(0.21)	(0.29)
ED_{555}		28.120427	65.113227	65.113227	95.934537	116.592792	116.592792	(0.21)	(0.29)
ED_{444}		28.121581	65.126966	65.126966	95.976800	116.667215	116.667215	(0.25)	(0.35)
TSPT	FG-O	23.5769	56.2107	56.2107	84.5669	104.1862	104.1862		
ED_{999}		23.584809	56.253273	56.253273	84.674705	104.318923	104.318923	(0.09)	(0.13)
ED_{888}		23.584811	56.253289	56.253289	84.674748	104.318999	104.318999	(0.09)	(0.13)
ED_{777}		23.585262	56.255337	56.255337	84.679783	104.324628	104.324628	(0.10)	(0.13)
ED_{666}		23.585263	56.255382	56.255382	84.680020	104.325230	104.325230	(0.10)	(0.13)
ED_{555}		23.590085	56.282635	56.282635	84.733460	104.414133	104.414133	(0.16)	(0.22)
ED_{444}		23.591566	56.289766	56.289766	84.750568	104.441178	104.441178	(0.18)	(0.25)
TSPT	FG-X	29.5212	65.7764	65.7764	95.6296	113.6785	113.6785		
ED_{999}		29.298234	64.882826	64.882826	94.097147	111.695680	111.695680	(1.42)	(1.74)
ED_{888}		29.298289	64.883200	64.883200	94.098072	111.697116	111.697116	(1.42)	(1.74)
ED_{777}		29.327575	65.003272	65.003272	94.309072	111.973745	111.973745	(1.23)	(1.50)
ED_{666}		29.327642	65.004469	65.004469	94.312719	111.979824	111.979824	(1.23)	(1.50)
ED_{555}		29.470211	65.587097	65.587097	95.331174	113.306257	113.306257	(0.29)	(0.33)
ED_{444}		29.471381	65.611470	65.611470	95.413238	113.448420	113.448420	(0.21)	(0.25)

Table 10: First 6 dimensionless frequency parameters of simply-supported UD and FG-GPLs reinforced composite plates with lay-out $[0/90]_{5T}$ and $T = 400\,\mathrm{K}$.

Theory	CNTs	Dimensionless circular frequency parameters							
		$\hat{\omega}_1$	$\hat{\omega}_2$	$\hat{\omega}_3$	$\hat{\omega}_4$	$\hat{\omega}_5$	$\hat{\omega}_6$	Ave. $\Delta\%$	Max $\Delta\%$
TSPT[51]	UD	21.9591	56.2626	56.2626	84.0641	103.2981	103.2981		
ED_{999}		21.930312	56.286968	56.286968	84.180379	103.494215	103.494215	(0.12)	(0.19)
ED_{888}		21.930312	56.286968	56.286968	84.180380	103.494218	103.494218	(0.12)	(0.19)
ED_{777}		21.930312	56.286968	56.286968	84.180380	103.494219	103.494219	(0.12)	(0.19)
ED_{666}		21.930312	56.286970	56.286970	84.180390	103.494252	103.494252	(0.12)	(0.19)
ED_{555}		21.930324	56.287304	56.287304	84.181779	103.497761	103.497761	(0.12)	(0.19)
ED_{444}		21.931771	56.302768	56.302768	84.227536	103.578080	103.578080	(0.17)	(0.27)
TSPT	FG-O	17.5580	48.0534	48.0534	73.9945	91.9321	91.9321		
ED_{999}		17.515004	48.017633	48.017633	73.990164	91.982600	91.982600	(0.08)	(0.24)
ED_{888}		17.515011	48.017660	48.017660	73.990227	91.982683	91.982683	(0.08)	(0.24)
ED_{777}		17.515334	48.018781	48.018781	73.993270	91.985309	91.985309	(0.08)	(0.24)
ED_{666}		17.515344	48.018796	48.018796	73.993411	91.985693	91.985693	(0.08)	(0.24)
ED_{555}		17.520974	48.044653	48.044653	74.046231	92.064109	92.064109	(0.10)	(0.21)
ED_{444}		17.523027	48.054034	48.054034	74.068268	92.100261	92.100261	(0.11)	(0.20)
TSPT	FG-X	23.8138	57.5307	57.5307	84.4584	101.8561	101.8561		
ED_{999}		23.654126	57.043178	57.043178	83.707980	100.926011	100.926011	(0.85)	(0.91)
ED_{888}		23.654163	57.043395	57.043395	83.708496	100.926818	100.926818	(0.85)	(0.91)
ED_{777}		23.663997	57.081608	57.081608	83.773569	101.013540	101.013540	(0.78)	(0.83)
ED_{666}		23.664011	57.082210	57.082210	83.775549	101.016983	101.016983	(0.77)	(0.82)
ED_{555}		23.746332	57.393828	57.393828	84.298713	101.691788	101.691788	(0.21)	(0.28)
ED_{444}		23.747571	57.418344	57.418344	84.378197	101.831914	101.831914	(0.14)	(0.28)

Table 11: First 6 dimensionless frequency parameters of simply-supported UD and FG-GPLs reinforced composite plates with lay-out $[0/90]_{5T}$ and $T = 500\,\mathrm{K}$.

Theory	CNTs	Dimensionless circular frequency parameters							
		$\hat{\omega}_1$	$\hat{\omega}_2$	$\hat{\omega}_3$	$\hat{\omega}_4$	$\hat{\omega}_5$	$\hat{\omega}_6$	Ave. $\Delta\%$	Max $\Delta\%$
TSPT[51]	UD	15.0774	48.7945	48.7945	74.6315	93.2513	93.2513		
ED_{999}		14.957112	48.714118	48.714118	74.612001	93.308594	93.308594	(0.21)	(0.80)
ED_{888}		14.957112	48.714125	48.714125	74.612006	93.308622	93.308622	(0.21)	(0.80)
ED_{777}		14.957112	48.714126	48.714126	74.612006	93.308625	93.308625	(0.21)	(0.80)
ED_{666}		14.957113	48.714133	48.714133	74.612023	93.308687	93.308687	(0.21)	(0.80)
ED_{555}		14.957133	48.714601	48.714601	74.613791	93.313337	93.313337	(0.21)	(0.80)
ED_{444}		14.959318	48.732900	48.732900	74.665213	93.402851	93.402851	(0.23)	(0.78)
TSPT	FG-O	9.8081	41.2808	41.2808	66.0908	83.5461	83.5461		
ED_{999}		9.622116	41.108755	41.108755	65.897340	83.401967	83.401967	(0.56)	(1.90)
ED_{888}		9.622120	41.108761	41.108761	65.897343	83.401983	83.401983	(0.56)	(1.90)
ED_{777}		9.622293	41.109092	41.109092	65.898402	83.402570	83.402570	(0.56)	(1.90)
ED_{666}		9.622294	41.109161	41.109161	65.898754	83.403303	83.403303	(0.56)	(1.90)
ED_{555}		9.635963	41.148050	41.148050	65.976630	83.511549	83.511549	(0.44)	(1.76)
ED_{444}		9.641306	41.162676	41.162676	66.008075	83.561940	83.561940	(0.41)	(1.70)
TSPT	FG-X	18.2245	51.1959	51.1959	76.4767	93.5499	93.5499		
ED_{999}		18.029082	50.812604	50.812604	75.970955	92.984839	92.984839	(0.74)	(1.07)
ED_{888}		18.029096	50.812699	50.812699	75.971178	92.985211	92.985211	(0.74)	(1.07)
ED_{777}		18.031349	50.820064	50.820064	75.982750	93.000519	93.000519	(0.72)	(1.06)
ED_{666}		18.031360	50.820539	50.820539	75.984253	93.003105	93.003105	(0.72)	(1.06)
ED_{555}		18.093911	51.020135	51.020135	76.301094	93.401687	93.401687	(0.32)	(0.72)
ED_{444}		18.095947	51.049547	51.049547	76.390034	93.557063	93.557063	(0.23)	(0.71)

Table 12: Critical buckling load $\lambda_{cr} = \sigma_{cr} \frac{b^2}{E_0 h^2}$ of a FG-GPLs reinforced composite plates $[0/90/0/90/0]_s$ with unloaded simply-supported edges at $T = 300\,\mathrm{K}$.

Theory	b/h	Critical Buckling load λ_{cr}					
		UD	Δ%	FG-X	Δ%	FG-O	Δ%
TSPT[51]	10	95.540		105.380		67.312	
ED_{999}		94.595296	(0.99)	102.714470	(2.53)	66.517539	(1.18)
ED_{888}		94.595296	(0.99)	102.714835	(2.53)	66.517548	(1.18)
ED_{777}		94.595297	(0.99)	102.920230	(2.33)	66.520081	(1.18)
ED_{666}		94.595297	(0.99)	102.920653	(2.33)	66.520084	(1.18)
ED_{555}		94.595355	(0.98)	103.923267	(1.38)	66.547117	(1.14)
ED_{444}		94.603119	(0.72)	103.930966	(1.37)	66.555708	(1.12)
TSPT[51]	20	105.073		120.995		71.198	
ED_{999}		104.750970	(0.31)	120.015985	(0.81)	70.960264	(0.33)
ED_{888}		104.750970	(0.31)	120.016109	(0.81)	70.960266	(0.33)
ED_{777}		104.750970	(0.31)	120.089336	(0.75)	70.961001	(0.33)
ED_{666}		104.750970	(0.31)	120.089361	(0.75)	70.961071	(0.33)
ED_{555}		104.750972	(0.31)	120.445177	(0.45)	70.968933	(0.32)
ED_{444}		105.252127	(0.17)	120.445927	(0.45)	70.974225	(0.31)
TSPT[51]	50	108.098		126.244		72.369	
ED_{999}		108.041274	(0.05)	126.067594	(0.14)	72.328892	(0.06)
ED_{888}		108.041270	(0.05)	126.067663	(0.14)	72.328894	(0.06)
ED_{777}		108.041276	(0.05)	126.080768	(0.13)	72.329016	(0.06)
ED_{666}		108.041274	(0.05)	126.080967	(0.13)	72.329128	(0.06)
ED_{555}		108.041275	(0.05)	126.144507	(0.78)	72.330444	(0.05)
ED_{444}		108.041291	(0.05)	126.149027	(0.75)	72.334883	(0.05)

Table 13: Critical buckling load $\lambda_{cr} = \sigma_{cr} \frac{b^2}{E_0 h^2}$ of a FG-GPLs reinforced composite plates $[0/90/0/90/0]_s$ with unloaded simply-supported edges at $T = 400\,\mathrm{K}$.

Theory	b/h	Critical Buckling load λ_{cr}					
		UD	Δ%	FG-X	Δ%	FG-O	Δ%
TSPT[51]	10	83.296		90.702		59.454	
ED_{999}		82.485577	(0.97)	89.106854	(1.76)	58.782003	(1.13)
ED_{888}		82.485577	(0.97)	89.107021	(1.76)	58.782037	(1.13)
ED_{777}		82.485577	(0.97)	89.162616	(1.70)	58.783361	(1.13)
ED_{666}		82.485577	(0.97)	89.162658	(1.70)	58.783392	(1.13)
ED_{555}		82.485639	(0.97)	89.629090	(1.18)	58.806586	(1.09)
ED_{444}		82.493230	(0.96)	89.635266	(1.18)	58.815620	(1.07)
TSPT[51]	20	92.094		104.218		63.340	
ED_{999}		91.813410	(0.30)	103.620992	(0.57)	63.134211	(0.32)
ED_{888}		91.813410	(0.30)	103.621051	(0.57)	63.134235	(0.32)
ED_{777}		91.813411	(0.30)	103.640751	(0.55)	63.134621	(0.32)
ED_{666}		91.813411	(0.30)	103.640955	(0.55)	63.134767	(0.32)
ED_{555}		91.813412	(0.30)	103.807100	(0.39)	63.141547	(0.31)
ED_{444}		91.814016	(0.30)	103.807884	(0.39)	63.146699	(0.30)
TSPT[51]	50	94.906		108.766		64.522	
ED_{999}		94.856366	(0.05)	108.658183	(0.10)	64.487027	(0.05)
ED_{888}		94.856366	(0.05)	108.658206	(0.10)	64.487053	(0.05)
ED_{777}		94.856366	(0.05)	108.661730	(0.10)	64.487113	(0.05)
ED_{666}		94.856366	(0.05)	108.662204	(0.10)	64.487316	(0.05)
ED_{555}		94.856366	(0.05)	108.691893	(0.07)	64.488453	(0.05)
ED_{444}		94.856383	(0.05)	108.696103	(0.06)	64.492620	(0.05)

Table 14: Critical buckling load $\lambda_{cr} = \sigma_{cr} \frac{b^2}{E_0 h^2}$ of a FG-GPLs reinforced composite plates $[0/90/0/90/0]_s$ with unloaded simply-supported edges at $T = 500\,\mathrm{K}$.

Theory	b/h	Critical Buckling load λ_{cr}					
		UD	Δ%	FG-X	Δ%	FG-O	Δ%
TSPT[51]	10	77.189		85.418		56.908	
ED_{999}		76.451333	(0.96)	84.207447	(1.42)	56.265917	(1.13)
ED_{888}		76.451333	(0.96)	84.207478	(1.42)	56.265923	(1.13)
ED_{777}		76.451335	(0.96)	84.217122	(1.41)	56.266299	(1.13)
ED_{666}		76.451335	(0.96)	84.217133	(1.41)	56.266299	(1.13)
ED_{555}		76.451409	(0.96)	84.486741	(1.09)	56.296996	(1.07)
ED_{444}		76.459232	(0.95)	84.494138	(1.08)	56.310170	(1.05)
TSPT[51]	20	85.889		98.572		60.973	
ED_{999}		85.627691	(0.30)	98.106590	(0.47)	60.773469	(0.33)
ED_{888}		85.627691	(0.30)	98.106593	(0.47)	60.773482	(0.33)
ED_{777}		85.627692	(0.30)	98.110100	(0.47)	60.773590	(0.33)
ED_{666}		85.627692	(0.30)	98.110308	(0.47)	60.773635	(0.33)
ED_{555}		85.627694	(0.30)	98.207932	(0.37)	60.782665	(0.31)
ED_{444}		85.628325	(0.30)	98.208269	(0.37)	60.790812	(0.30)
TSPT[51]	50	88.693		103.024		62.219	
ED_{999}		88.646194	(0.05)	102.939269	(0.08)	62.185109	(0.05)
ED_{888}		88.646191	(0.05)	102.939269	(0.08)	62.185127	(0.05)
ED_{777}		88.646192	(0.05)	102.939901	(0.08)	62.185147	(0.05)
ED_{666}		88.646194	(0.05)	102.940334	(0.08)	62.185224	(0.05)
ED_{555}		88.646196	(0.05)	102.957867	(0.06)	62.186742	(0.05)
ED_{444}		88.646212	(0.05)	102.960853	(0.06)	62.193562	(0.04)

Figures

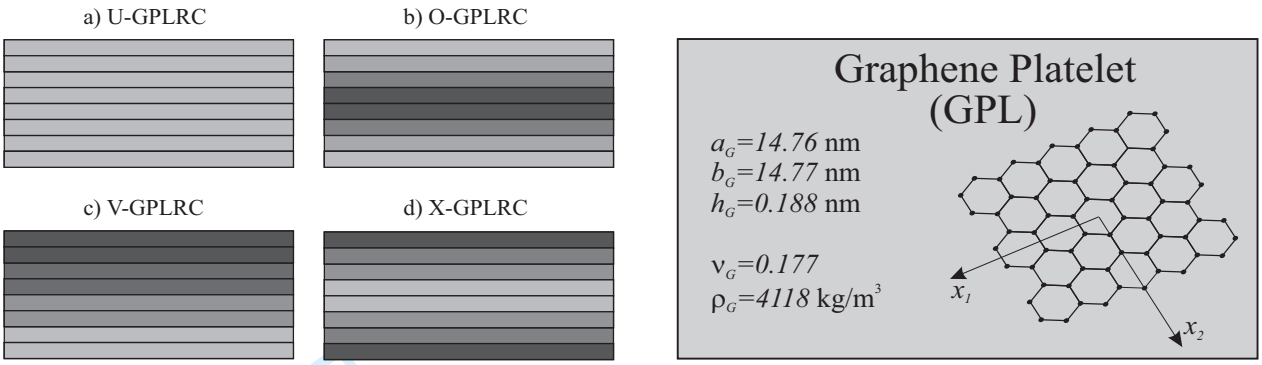

Figure 1: Graphene nanoplatelet-reinforced composite (GPLRC) plate configurations.